From the division of Medical Engineering,
department of Laboratory Medicine,
Karolinska Institutet, Stockholm, Sweden

SKIN CANCER AS SEEN BY ELECTRICAL IMPEDANCE

Peter Åberg

Stockholm 2004

© Peter Åberg 2004
ISBN 91-7140-103-2

ABSTRACT

This thesis describes the relation between skin cancer and electrical impedance. On the cellular level, electrical impedance measured at clinically relevant frequencies is affected by e.g. membrane structure and orientation, and composition of and relation between the intra- and extracellular environments, i.e. similar properties used by histopathologists to diagnose skin cancer. The aim is to detect skin cancer using the electrical impedance technique. The overall objective is to develop a complement to visual skin cancer screening.

Impedance was measured with a depth selective impedance spectrometer between 1 kHz and 1 MHz of various skin cancers and benign lesions including e.g. malignant melanoma, squamous and basal cell carcinoma, dysplastic nevi, actinic keratosis, and benign pigmented nevi. The lesions were subsequently excised and diagnosed by histopathology. Various pattern recognition tools were used to analyse the impedance data.

First of all it was concluded that impedance of lesions differs from healthy skin, which confirms previous publications. It was also concluded that healthy skin varies within small areas on the body, which is a factor, amongst others, that might lower the signal-to-noise ratio of skin cancer impedance. Extensive measurements with a new version of the impedance spectrometer facilitated separation between skin cancer and benign nevi with clinically relevant accuracy. To improve the signal-to-noise ratio, a novel type of electrode that penetrates the outermost layer of the skin was introduced, and it was found that the accuracy varies with electrode and cancer type. Area under ROC curve was 91% for the separation of nevi and melanoma, and 98% for nevi and basal cell carcinoma.

The results strongly suggest that the electrical impedance technique can be used to detect skin cancer, i.e. proof-of-principle has been achieved. However, before the technique can be used as a routine instrument in the clinics, additional studies are required.

Keywords: electrical impedance, skin cancer, pattern recognition, screening

LIST OF PUBLICATIONS

This thesis is based on the following papers, referred to by their roman numerals.

I P. Åberg, P. Geladi, I. Nicander, and S. Ollmar, "Variation of skin properties within human forearms demonstrated by non-invasive detection and multi-way analysis," *Skin Res Technol*, vol. 8, pp. 194-201, 2002.

II P. Åberg, I. Nicander, U. Holmgren, P. Geladi, and S. Ollmar, "Assessment of skin lesions and skin cancer using simple electrical impedance indices," *Skin Res Technol*, vol. 9, pp. 257-61, 2003.

III P. Åberg, I. Nicander, J. Hansson, P. Geladi, U. Holmgren, and S. Ollmar, "Skin cancer identification using multi-frequency electrical impedance – a potential screening tool," *IEEE Trans Biomed Eng*, in press.

IV P. Åberg, I. Nicander, and S. Ollmar, "Minimally invasive electrical impedance spectroscopy of skin exemplified by skin cancer assessments," in *Proceedings of the 25th Annual International Conference of the IEEE Engineering in Medicine and Biology Society, Vols 1-4 - a New Beginning for Human Health*, vol. 25, *Proceedings of Annual International Conference of the IEEE Engineering in Medicine and Biology Society*. New York: IEEE, 2003, pp. 3211-3214.

V P. Åberg, P. Geladi, I. Nicander, J. Hansson, U. Holmgren, and S. Ollmar, "Non-invasive and microinvasive electrical impedance spectra of skin cancer - a comparison between two techniques," *Skin Res Technol*, submitted.

CONTENTS

LIST OF ABBREVIATIONS

ANOVA	analysis of variance
AUC	area under curve
BCC	basal cell carcinoma
CPE	constant phase element
EIT	electrical impedance tomography
FN	false negative
FP	false positive
IMIX	imaginary part index
LDA	linear discriminant analysis
MEMS	micro-electro-mechanical systems
MIX	magnitude index
MM	malignant melanoma
NMSC	non-melanoma skin cancer
NPV	negative predictive value
PARAFAC	parallel factor analysis
PCA	principal component analysis
PIX	phase index
PPV	positive predictive value
RIX	real part index
ROC	receiver operating characteristics
SB	SciBase
SC	stratum corneum
SCC	squamous cell carcinoma
SE	standard error
TEWL	trans epidermal water loss
TN	true negative
TP	true positive

1 BACKGROUND

THE experience of the group working with electrical skin impedance is that everything that can be seen histologically in a microscope can be measured with electrical impedance. What you see in a microscope is mainly structural properties of the tissue, such as size, shape and orientation of the cells, amount of intra and extra cellular water, and structure of the cell membranes. These structural properties are to a high degree reflected in the impedance spectra. Skin cancers and other lesions are histologically diagnosed based on their unique cell structures, and hence, clinically (histopathologically) relevant skin cancer information can be found in multi-frequency electrical impedance spectra. The aim of this thesis is to describe how this information can be extracted from the impedance, and how it can be used to distinguish harmful and harmless skin lesions.

1.1 ELECTRICAL IMPEDANCE

ELECTRICAL impedance is measure of a material's opposition to the flow of electric current. Impedance includes both resistance and reactance, and, according to Encyclopædia Britannica Online [6], "*The resistance component arises from collisions of the current-carrying charged particles with the internal structure of the conductor. The reactance component is an additional opposition to the movement of electric charge that arises from the changing magnetic and electric fields in circuits carrying alternating current.*" Electrical impedance, Z, is the ratio between alternating voltage and alternating current, described by Ohm's law. Impedance is a complex measure of the resistance, R (ohm), and reactance, X (ohm), as shown in figure 1, that can be expressed in the complex impedance plane according to $Z = R + iX$, or in polar coordinates using the magnitude, $|Z|$ (ohm), and phase, θ (deg), according to $Z = |Z|e^{i\theta}$, where $|Z| = (R^2 + X^2)^{0.5}$, and $\theta = \arctan(X/R)$.

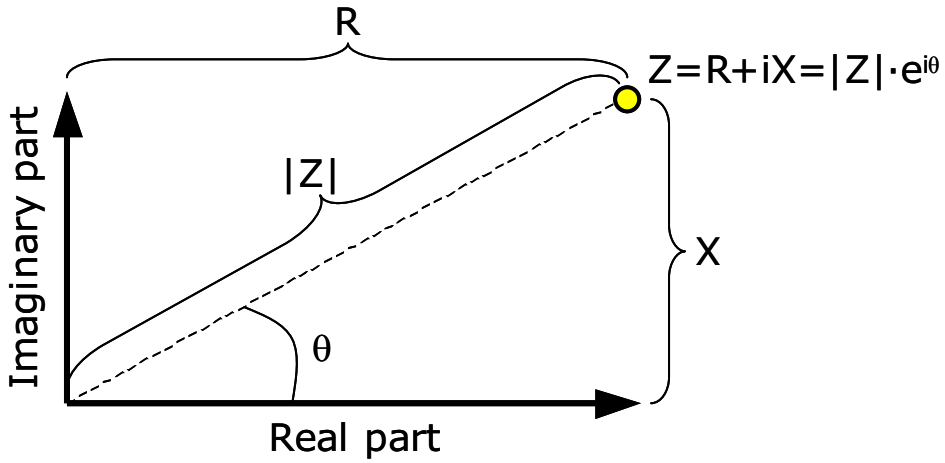

Figure 1. Plot of the electrical impedance, Z, as coordinates of resistance, R, and reactance, X, in the complex impedance plane. Impedance can be expressed in polar coordinates using the magnitude, |Z|, and phase, θ.

1.1.1 Electrical bio-impedance

The membrane around living cells acts like an electrochemical membrane, i.e. it is semi-permeable and allows certain ions to pass through the membrane and others not. This makes the membrane behave like a leaky capacitor. Moreover, the intra- and extracellular environments consist mainly of electrolytes and have primarily resistive properties. Thus, cell suspensions and biological tissues have both capacitive and resistive properties, and impedance of biological tissues are highly frequency dependent. Different biomaterials have different electrical properties – tissue structure and chemical composition of a biological material may correlate with its electrical properties, and thus bio-materials have different frequency characteristics [7]. Generally, the low-frequency region is affected by the extracellular environment and high frequencies also by the properties of the intracellular space, demonstrated in figure 2. Since cell membranes have a high capacitance, low frequency currents and dc currents must pass around the cells, i.e. they travel in the extracellular environment. High frequency currents, on the other hand, have the ability to penetrate through cell membranes and other electronic barriers in the cell structure by polarisation, i.e. the barrier is charged, uncharged, and reversely charged, and so on, like a simple capacitor. Thus, different frequency regions are affected by different fundamental properties of the tissue.

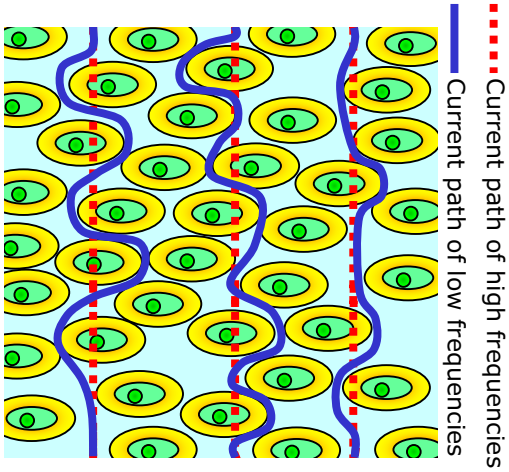

Figure 2. Paths of high and low frequency currents in a biological material. Low frequency currents travel in the extracellular environment, whereas the high frequency currents penetrate the cell membranes and go through both the intra- and extracellular environments.

Electrical impedance spectra of biologic materials contain frequency regions where the impedance decreases with increased frequency, and others where the impedance is almost constant, shown in figure 3. The regions where the impedance decreases with frequency, i.e. the steep slopes in figure 3, corresponds to specific electrochemical processes or phenomena, called dispersions. Bio-impedance spectra plotted in a Nyquist diagram, i.e. a plot of real vs. imaginary part of the impedance, displays sections of semicircles, and each semicircle corresponds to a specific dispersion. Schwan was the first to correctly identify three major dispersions of electro bio-impedance spectra in 1957 [8], the α-, β- and γ-dispersions, visualised in figure 3. The α-dispersion (Hz to tens of kHz) reflects mainly polarisation of ionic clouds around the cells. Structural membrane changes, oedema, and polarisation of cell membranes affect the β-dispersion (kHz to hundreds MHz). The γ-dispersion (over hundreds MHz) reflects relaxation of water and other small molecules. Hence, the β-dispersion often contains most of the clinically relevant information. Later on, a fourth dispersion, called the δ-dispersion, was discovered in the lower GHz region.

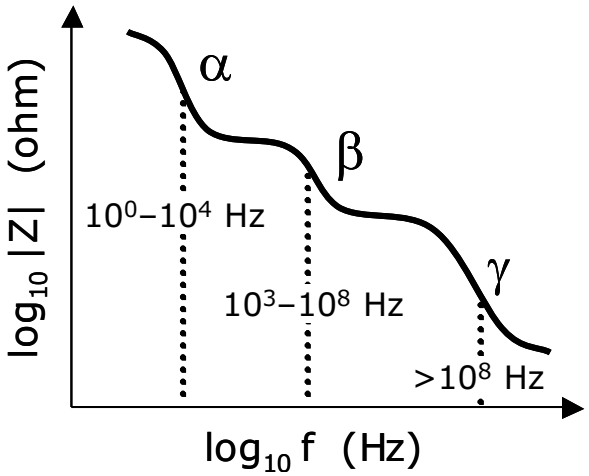

Figure 3. Schematic figure of the frequency dependence and dispersive characteristics of the magnitude of electrical impedance of a simple biological material.

Electrical impedance of biological materials is thoroughly reviewed in [9], where the major contributors are exposed historically along with some examples of impedance applications. Apart from the skin cancer impedance assessments, there are not many examples of applications where the bio-impedance is used clinically: it is used e.g. to evaluate body composition, to make impedance images, and to detect caries. Whole body electrical bio-impedance is correlated to various body composition parameters, such as total body water, fat free mass, and body fat, and the technique is used as a routine instrument for total body composition analysis and evaluation of nutritional status [10]. Electrical impedance tomography (EIT) is an imaging technique that is mainly used for research, reviewed by Brown in [11], and impedance measurements of teeth can be used to detect caries, described in [12].

1.1.2 Skin impedance

Generally, human skin consists of two layers, epidermis and dermis, described in [13]. The main function of the lower layer, dermis, is to provide the skin with mechanical strength and elasticity. Thickness of this layer varies between 0.3 mm to a couple of millimetres. The dermis has a complex structure and contains e.g. connective tissue, blood vessels, hair follicles, sensory nerves, and sweat glands.

Epidermis is the outer layer. This layer is thin, typically around 0.05-0.5 mm (the thickness varies with location), and acts as a barrier against

radiation, microbes, and chemicals, especially water. Epidermis is composed of closely packed cells with small amounts of extracellular water. Cells in epidermis keratinise, become more and more flattened, and migrate closer to the surface over time. When the cells reach the outermost layer of epidermis, the stratum corneum (SC), they are scaly and compressed, and in the end they fall off. Hence, the epidermis and the SC are constantly renewed. The thickness of the SC varies to a large extent with body site, and the average thickness is approximately 15 μm.

A typical non-invasive electrical impedance spectrum of healthy skin is shown in figure 4. The complex impedance in the Nyquist plot in figure 4b resembles a straight line, at least in the low frequency region from 1 kHz up to about 100 kHz, which implies that impedance of skin with intact SC can be approximated by linear regression, or described by only two frequencies, without loosing too much information, discussed in section 1.2.1.2.

Non-invasive impedance of skin is dominated by the very high impedance of the stratum corneum, specially in the low-frequency region up to some kHz [9]. Stripping the skin with common adhesive tape, described in [14], removes stratum corneum cells and hence lowers the skin impedance [15]. If stratum corneum cells are removed, the dispersion of the underlying skin layer is accentuated, i.e. impedance spectrum of stripped skin has different shape and is much lower than skin with intact SC [16, 17]. This is exemplified in figure 5, where skin of a healthy volunteer was measured

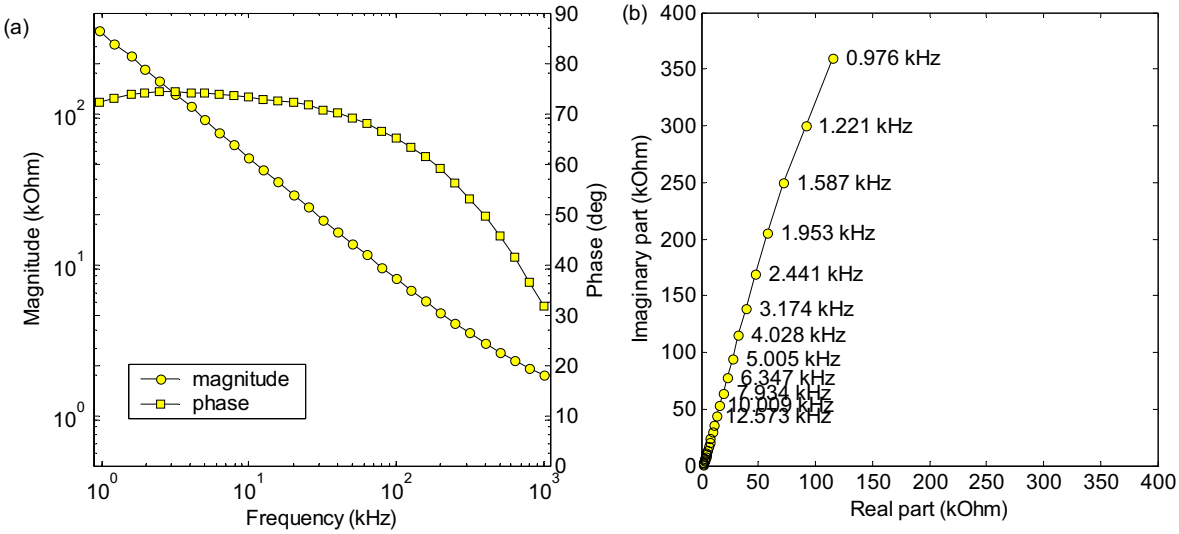

Figure 4. Bode plot of a typical non-invasive impedance spectrum of normal skin (a), and the corresponding Nyquist plot of the complex impedance (b).

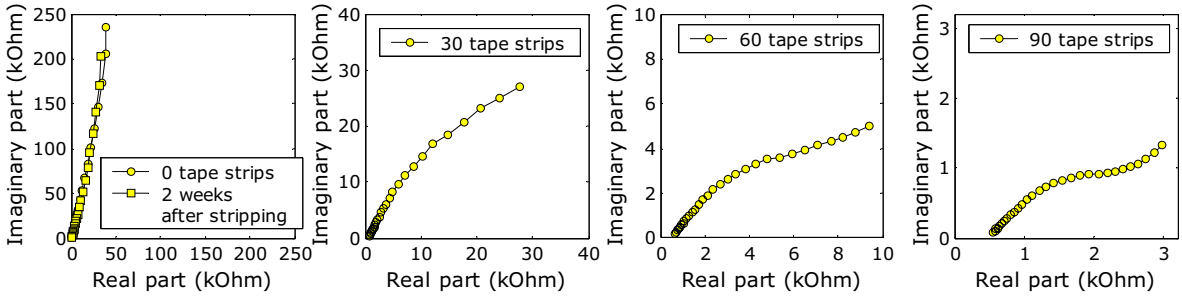

Figure 5. Nyquist plots of impedance spectra (1.22 kHz to 1 MHz) before tape stripping, and after 30, 60, and 90 tape strips. Two weeks after the tape stripping the skin of the healthy volunteer was recovered.

before, during, and 2 weeks after tape stripping with common adhesive tape. It can be seen that the impedance decreases with the number of strips, and that the graphs gradually takes on the shape of a section of a semicircle. After stripping the skin with 90 tape strips, sections of two different semicircles were discernible, which implies that the α- and β-dispersions of viable skin are uncovered when removing the SC. The skin was fully recovered after two weeks.

It is evident that the status of the SC dominates the non-invasive impedance of human skin, and impedance can thus be used to evaluate the status of the barrier function of skin, e.g. by assessing skin hydration and oedema. Skin hydration is an essential parameter for the barrier function of skin that modulates the electrical properties of the SC [17, 18]. Oedema, is one result of skin irritation, characterised by excessive amount of watery fluid accumulated in the extracellular environment, can easily be detected by electrical impedance in the α- and β-dispersion regions. This can be explained in terms of current paths of high and low frequency currents through tissues with closely packed cells (e.g. healthy normal skin) and

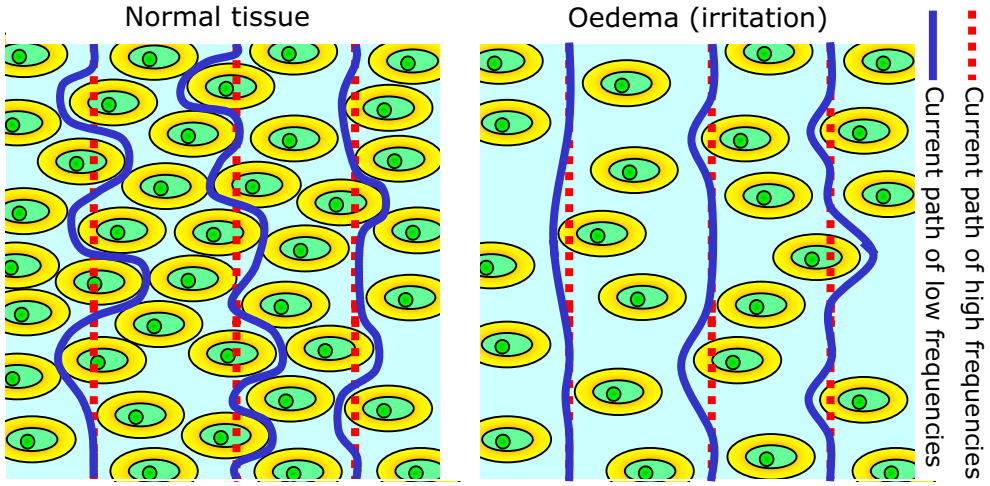

Figure 6. Paths of high and low frequency currents in normal and irritated tissues.

tissues with oedema (e.g. irritated skin), exemplified in figure 6. For the high frequencies, the impedance of normal tissue is similar to the impedance of oedema. For lower frequencies, on the other hand, where currents mainly travel in the extracellular environment, the impedance of the normal tissue is much higher than the oedema. Electrical impedance has previously been used to characterize and quantify reactions in skin [19-23]. Skin impedance can also be used to e.g. map baseline properties of healthy skin [24-30], and to assess skin diseases [31, 32]. Electrical impedance measurements of skin originates from Gildemeister [33] almost 100 years ago. Reviews on electrical impedance of skin can be found in [16, 17, 34].

1.1.3 Non-invasive and microinvasive impedance

Non-invasive impedance of skin can be measured between two electrodes, a two-point measurement, by applying a small alternating voltage and comparing the measured current with the voltage according to Ohms law. Depth penetration of the currents in skin and other biological material is correlated to frequency, distance between and size of the electrodes, and physical properties of the tissue under study, in particular the multi-layered structure with different electrical properties. A rule of thumb is that depth penetration of the currents within the layers of the skin are roughly half the distance between the electrodes, as demonstrated in figure 7. High frequencies penetrate deeper than lower frequencies in a double layer structure where the top layer is less conductive and more capacitive than the deeper layer.

The relation between depth penetration and distance between electrodes can be used to make a depth selective skin impedance meter. The principle

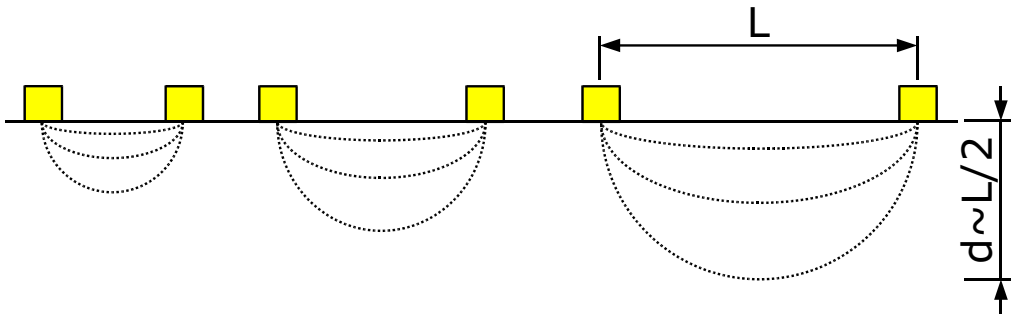

Figure 7. Current lines in a biological tissue from electrode systems with varying distance between the electrodes demonstrate that depth penetration of the currents are approximately half the distance between the electrodes.

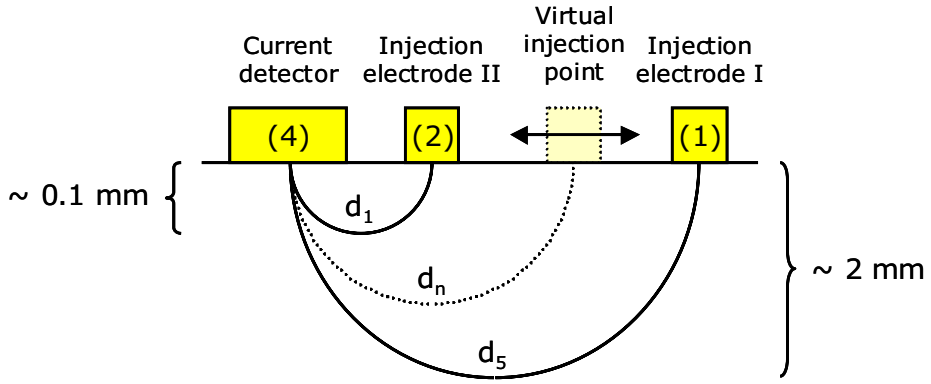

Figure 8. The principle of the depth selectivity where the ratio between voltages at the injection electrodes determines the depth penetration.

of the SciBase (SB) depth selective non-invasive impedance probe is shown in figure 8. The non-invasive probe consists of a concentric ring system. The rings represent voltage drive (current injection) points, current detector, and a guard ring. The voltage drive supplies a small, not noticeable, alternating voltage in the tissue, and the detector measures the resulting current. The guard ring eliminates currents on the surface of the tissue, e.g. in the surface furrows of the skin, which otherwise can cause artefacts. There are two rings that supply voltage, and the relation between the two will generate a virtual injection point located between the two. Adjusting the voltage relation between the two injection points will move the virtual injection back and forth, and hence the depth penetration in the tissue is selectable. The currents from the SB instrument equipped with the non-invasive probe penetrate the skin in five steps approximately between 0.1 and 2 mm into the epidermis and dermis. The electrode system on the tip of the non-invasive probe is shown in figure 9, and the whole handheld probe is shown in figure 10.

The Thévenin's theorem and the principle of superposition tell us that any linear system can be expressed as an algebraic sum of individual contributions. This implies that all depth settings can be calculated from two

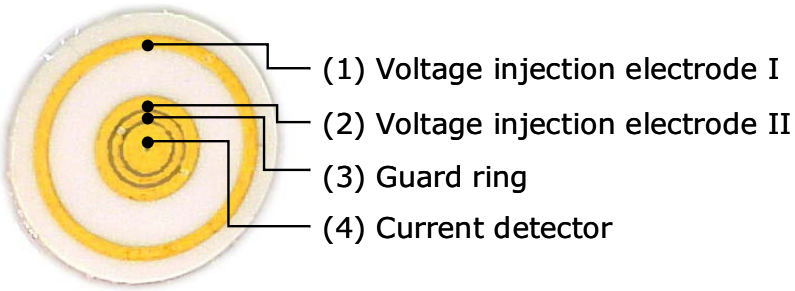

Figure 9. The electrode ring system on the tip of the non-invasive probe.

Figure 10. The non-invasive probe.

measurements for any electronically linear system, i.e. all depth related information could be achieved from only two observations of the tissue, and multiple depth measurements are only linear combinations of each other. However, human skin is a complex, heterogeneous, and anisotropic multilayer structure with electronically non-linear properties. The most non-linear properties are located to the SC, which does not obey the Cole-equation [35]. Therefore, there is information in all depth measurements that cannot be calculated by interpolation or extrapolation from two depths, although the different depths are highly correlated.

As pointed out previously, non-invasive electrical impedance spectra of skin are dominated by the dielectric properties of the stratum corneum, especially at low frequencies. The stratum corneum has a very large and broad α-dispersion that overshadows the α- and β-dispersions of the underlying viable skin, i.e. the physical information of the dispersions is confounded, and the clinically relevant information from the viable skin is thus diluted. This makes it difficult to assess electrical impedance of phenomena that manifest below the stratum corneum, e.g. skin cancer and allergic reactions, while other phenomena, such as skin irritations, that affect both the stratum corneum and the viable skin below, and barrier damage that only affects the SC, will be assessable using regular non-invasive electrical skin impedance. One way to access electrical impedance of the viable skin beneath the SC is, as described above, to remove the SC with e.g. tape stripping. Another possibility is to penetrate the SC and measure

the impedance below using dedicated electrodes with micro-spikes, demonstrated by Griss et al. in [36]. They made the micro-needles in silicon using micro-electro-mechanical systems (MEMS) techniques. Subsequently, depth selective impedance electrodes with micro-needles were developed for the SB spectrometer, as shown in figure 11. The surface of the electrodes is covered with gold, and the spikes are approximately 150 µm long and 30 µm in diameter. The spiked electrodes are mounted onto a handheld probe, as shown in figure 12. The probe has three beams furnished with spikes – one beam is for current detection and the other two are drive electrodes facilitating depth selectivity according to the same principle as the regular non-invasive probe. There is no need for a guard electrode because there are no disturbing currents on the surface of the skin in this case. The area of the electrode is approximately 5 x 5 mm^2. The spikes are designed to penetrate through stratum corneum, but not into the dermis (unless excessive pressure is applied), and the spiked electrode is, by definition, not non-invasive, but since the spikes do not reach the blood vessels or the sensory nerves in dermis, we classify the probe as microinvasive. Measurements with the micro-invasive electrodes are painless (a measurement feels like holding a piece of sandpaper to the skin), and it is harmless as long as the spikes are clean. The electrodes are used as disposables. The terms 'minimally invasive probe', 'micromally invasive probe', 'spike probe', and 'spiked probe' used in previous publications, e.g. [37, 38] and in papers **III** and **IV**, are different names of the same microinvasive electrode system.

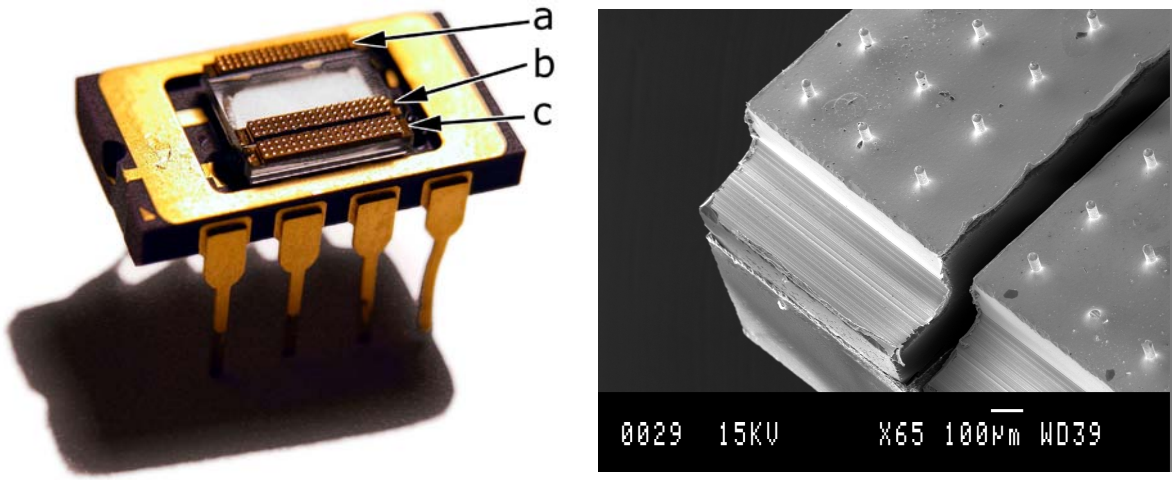

Figure 11. The electrode system of the microinvasive probe (left), and a close-up of the spikes on the surface (right). The voltage is applied at the beams marked (a) and (b), and the current is detected in beam (c). The spikes are approximately 150 µm long and 30 µm in diameter.

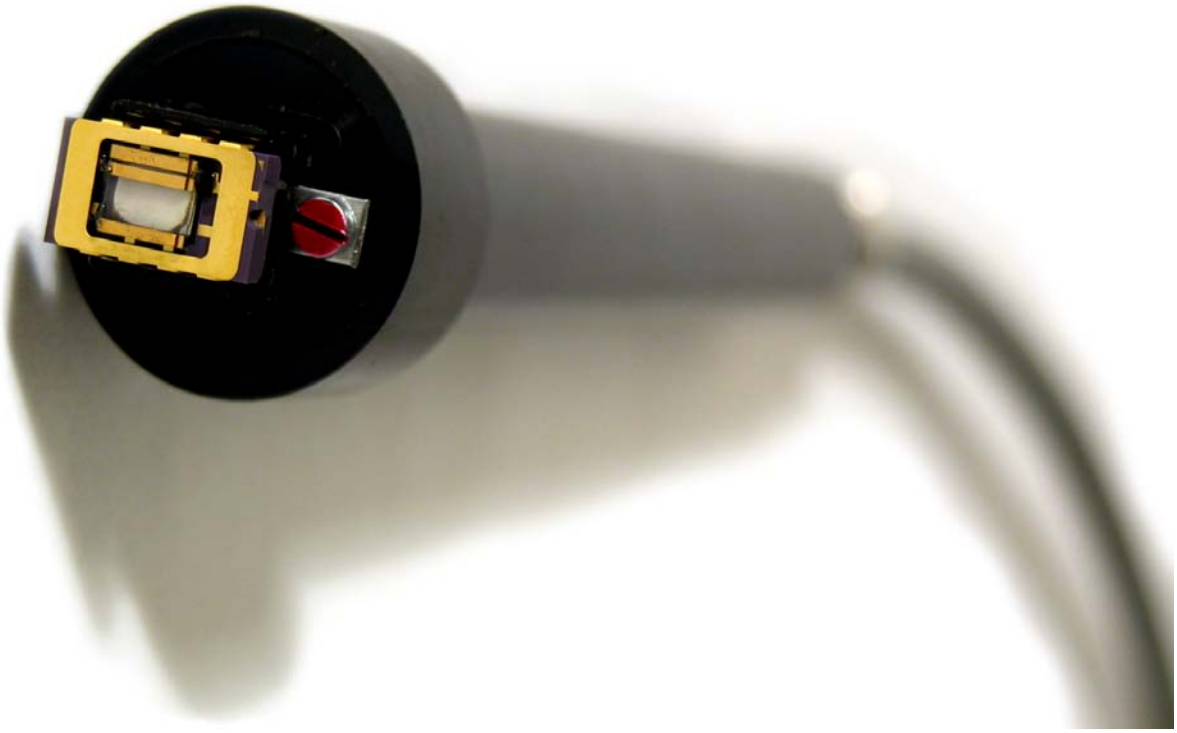

Figure 12. The spiked microinvasive probe.

Skin impedance measured non-invasively is affected by many biological factors, such as gender, age and body location, that dilute the clinically relevant information from the tissue under study. Thus, this biological variation is a drawback when the impedance technique is used in skin investigations, and in particular when subtle skin phenomena are under study. The biological variations are typically dominating in the outermost layer of the skin, and eliminating the SC with the microinvasive electrodes would therefore reduce biological variations and enhance the clinically relevant signals from the viable skin. This is of special interest when assessing phenomena that are located beneath the SC layer, e.g. phenomena that do not affect the SC, such as early stage malignant melanoma and allergic reactions.

1.1.4 Skin cancer

There are different skin cancer types, where malignant melanoma (MM), basal cell carcinoma (BCC), and squamous cell carcinoma (SCC) are the most significant [39-44]. BCC and SCC are called non-melanoma skin cancers (NMSC) [45]. Actinic keratosis can progress to SCC [46], and hence is considered as a potentially harmful lesion type. The benign pigmented

nevus, on the other hand, is a harmless and very common lesion type. Dysplastic nevi are lesions with atypical features, and has an increased risk of progressing to MM [47]. Seborrheic keratosis is one of the most common benign skin lesions in adults [48]. Dermatofibromas are benign lesions that can develop after e.g. a viral infection or an insect bite [13, 49]. Benign lesions, such as pigmented nevi and seborrheic keratoses, can be mistaken for MM, and are therefore often excised for diagnostic purposes. Dysplastic nevi may be confused with both MM and benign nevi. A reduction of the number of benign lesions excised is economically motivated and would e.g. reduce discomfort and the risk of infections for the patients.

Screening for skin cancer is usually made by visual inspection of the lesions using e.g. the ABCD rule for MM [50], and atypical lesions are excised and examined histopathologically. The clinical accuracy of the screening ranges from poor to fair [51]. It is desirable to replace this subjective procedure with a non-invasive, reliable, simple, and objective technique with high accuracy, but at the time of writing there are no practical alternatives. Electrical impedance has been used to assess skin cancer with positive outcome and it has been proposed that electrical impedance could be used as a possible alternative to visual screening for skin cancer [52-57].

1.2 NUMERICAL ANALYSIS OF IMPEDANCE DATA

THE major problem when analysing bio-impedance spectra is that the data are multivariate and the impedance is complex, i.e. all depth settings and frequencies are correlated to each other, and each data point is represented by two numbers i.e. magnitude and phase, or real and imaginary part. When analysing impedance data there are often many variables (an impedance spectrum measured with the SB impedance spectrometer generate 310 highly correlated variables), which implies that it is ambiguous to perform univariate analysis of each variable, i.e. to analyse one variable at a time, because of the information redundancy. Furthermore, it is not obvious how to analyse complex numbers numerically. In order to interpret bio-impedance spectra, it is necessary to fit the raw data in a model or, in some other way, to simplify the data to a few clinically relevant parameters. When the data are simplified, post-

processing is often required, e.g. classical statistical analysis or classification. Numerical classification of skin lesion impedance spectra is of special interest in this thesis.

Some of the numerical tools described in this section are based on projections of data from multivariate dimensions to lower sub-spaces. Such methods are best described with linear algebra. In linear algebra, bold capital letters, **X**, means matrices, and bold lower-case letters, **x**, means vectors. Transposed data structures are marked with an apostrophe, e.g. **x**′. Multi-way data arrays are indicated with bold underlined capital letters, $\underline{\mathbf{X}}$ [58].

1.2.1 Parameterisation techniques

Four feature extraction techniques that are relevant for the analysis of impedance data will be described in this section: Cole-Cole modelling, impedance indexation, principal component analysis (PCA), and parallel factor analysis (PARAFAC). Cole-Cole modelling is a semi empirical approach that focuses on the dielectric behaviour of materials. Basically, the intention is to find equivalent electronic circuits with properties that resemble the material under study. The outcome of the Cole-Cole models is a set of simple electronic elements, i.e. Cole-Cole modelling is a reduction of impedance spectra to a handful lumped parameter electronic components. The indexation is an empirical approach, and the indices are based on the ratio between impedance at low and high frequency. It is a simple and straightforward method, and the indices are efficient in monitoring damages in stratum corneum, such as skin irritations that distort impedance spectra heavily. However, there are other numerical approaches, such as PCA and PARAFAC, that capture more information from the whole impedance spectra, which are more appropriate when studying subtle phenomena. PCA and PARAFAC are based on linear projections of data to lower subspaces.

1.2.1.1 Cole-Cole modelling

Traditionally, bio-impedance of a dispersion has been fitted to Cole-Cole-type equivalent circuits, virtual electronic circuits that fit the measured impedance spectra [9]. From the equivalent circuits it is possible to extract

empirically absolute values, such as membrane conductivity, and resistance of the extra- and intracellular environments (figure 13), provided the model is a reasonable description of the tissue.

According to Cole [59], bio-impedance, Z, is a function of frequency, f, which can be approximated by the Cole-Cole equation, given by:

$$Z(f) = R_\infty + \frac{R_0 - R_\infty}{1 + \left(\mathrm{i}\frac{f}{f_c} \right)^{1-\alpha}},$$

where f_c (Hz) is the characteristic frequency of the actual dispersion. R_0 and R_∞ (ohm) are resistances at low and high frequency, respectively. The α is a constant that, to some degree, reflects the heterogeneity of the tissue. The α attains a value between zero and 0.5, where zero represents a very homogeneous tissue.

In practice, Cole-Cole approximation is basically curve-fitting of experimentally measured impedance to a semi-circle arc in the complex impedance plane, visualised in figure 14. The Cole-equation is solved using, for example, a least-square deviation method, or any other appropriate numerical method.

The Cole-Cole model reduces a complex impedance spectrum to four parameters with physical units, and it is possible to interpret the Cole-

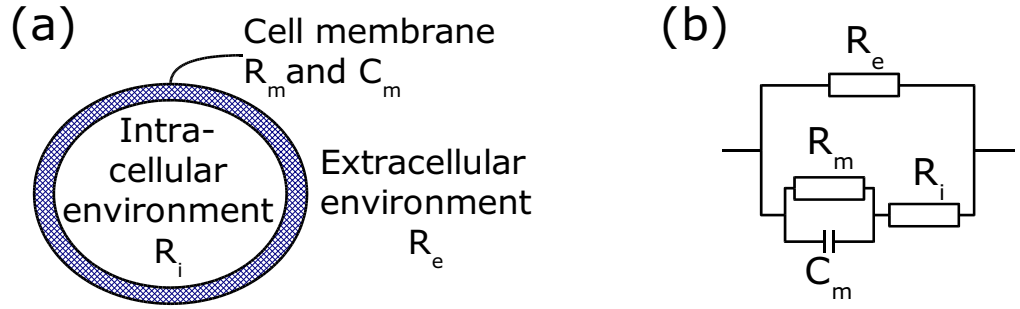

Figure 13. (a) A cell with electrical elements that correspond to the resistance of the extra- and intracellular environments, R_e and R_i, respectively, and resistance and capacitance of the cell membrane, R_m and C_m, respectively. (b) A simplistic equivalent circuit that corresponds to the properties of the cell in the β-dispersion frequency range.

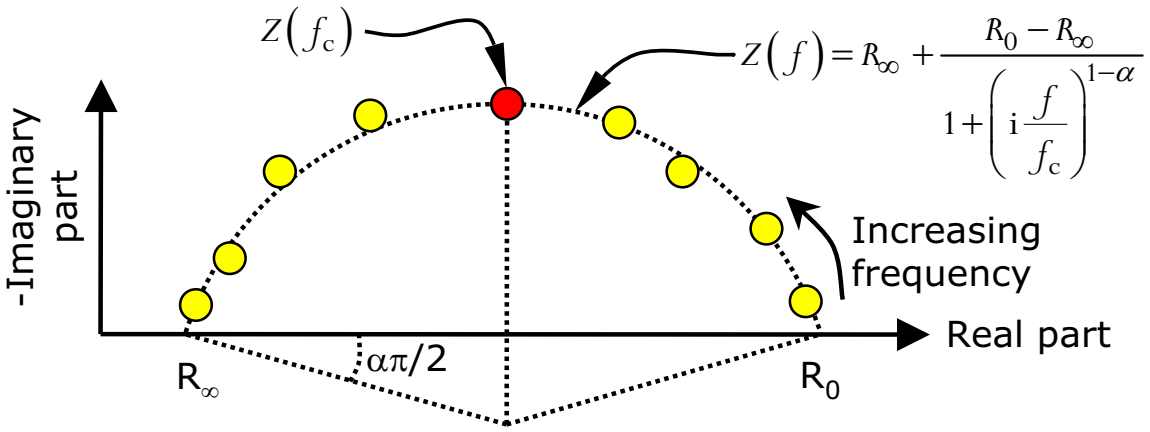

Figure 14. Cole-Cole approximation of measurements in the complex impedance plane.

parameters as physical properties of the biological tissue. A change of α, for example, is interpreted as a homogeneity change of the tissue under study.

The Cole-Cole equation is a simple model valid for one dispersion with characteristic frequency f_c. It is possible to extend the model to fit the three fundamental dispersions (the α-, β-, and γ-dispersions), so called multiple Cole systems [9]. However, this basic multiple Cole model will return 12 Cole parameters (4 parameters for each dispersion). The multiple Cole model can be extended to fit real life skin impedance spectra by adding more virtual electrical components that corresponds to specific elements in the Cole-Cole equations. As mentioned in section 1.1.2, skin contains layers (epidermis and dermis) and several sub-layers (e.g. stratum corneum), and each layer contains a set of fundamental dispersions. Hence, a multiple Cole model of three skin layers will generate at least 36 Cole parameters. Moreover, including additional Cole elements that correspond to e.g. electrode polarisation, sweat ducts, and deeper tissue, will increase the complexity of the multiple Cole model even further. Of course, it is possible to simplify the model of skin impedance by using some assumptions, but the point is: the more elements included in the model, the more variables will come out of the equations, and the f_c, R_0, R_∞, and α of the different dispersions are not necessarily independent of each other, i.e. they might be redundant. Thus a multiple Cole model is not necessarily an efficient data reduction tool, and the outcome of a multiple Cole model is still a multivariate data set with possible high inherent cross-correlation. By adjusting the Cole equivalent circuits, e.g. introducing additional fictive electronic components, like the so called constant phase elements (CPE), it is always possible to get at good fit between experimental values and

mathematical equations. However, good fit between measured impedance spectra and a multiple Cole model is *not* a proof that the theoretical assumptions behind the model are correct. Yamamoto and Yamamoto [35] described that the SC does not obey the Cole-equation, discussed in [18], which implies that it is ambiguous to fit non-invasive electrical impedance of skin with intact SC to any Cole model. Nevertheless, Cole-models have been widely used to simplify bio-impedance spectra of various tissue types, including skin with intact stratum corneum, often without adequate justification of the chosen model.

1.2.1.2 Impedance indexation

A Nyquist plot of non-invasive impedance of healthy skin with intact stratum corneum in the β-dispersion region is close to a straight line (exemplified in figure 4b). The squared correlation coefficient, r^2, of linear relation between real and imaginary parts of non-invasive skin impedance with intact stratum corneum typically varies between 98% and 100%. This implies that two points will capture most of the variance in a spectrum. Ollmar and Nicander [60] introduced four impedance indices – magnitude index (MIX), phase index (PIX), real part index (RIX), and imaginary part index (IMIX) – given by the relation between impedance at low (20 kHz) and high frequencies (500 kHz), according to:

$$\begin{aligned} MIX &= |Z_{20\,kHz}| \;/\; |Z_{500\,kHz}| \\ PIX &= \theta_{20\,kHz} - \theta_{500\,kHz} \\ RIX &= R_{20\,kHz} \;/\; |Z_{500\,kHz}| \\ IMIX &= X_{20\,kHz} \;/\; |Z_{500\,kHz}| \end{aligned}$$

The impedance indices have shown to be very effective when describing various skin conditions and phenomena, especially skin irritations that affect the barrier function of the SC. It was concluded in [19, 61, 62] that skin-irritations show unique index-patterns. Using the indices and numerical pattern recognition it was proposed that non-invasive skin impedance measurements could be used as a diagnostic decision support tool for various types of skin-related diseases. It was also found that the detection limit of the indices was lower than traditional visual scoring [20]. However, using holographic neural networks [63], it was found that there is additional information in the spectra not captured by the four indices. This implies

that, in the case subtle skin impedance changes are to be found, the indices are not powerful enough to capture all available biological information and it requires more powerful data-mining techniques, e.g. artificial neural networks and multivariate data analysis, discussed in [64]. Moreover, the indices depend on each other, e.g. according to $MIX^2 = RIX^2 + IMIX^2$, discussed in [65], and hence they describe redundant information.

Real vs. imaginary part of impedance spectra of the viable skin below the SC is not linear and do not fit very well to a straight line. The impedance indices do not account for the dispersive properties of the viable skin, and thus the indices will miss significant clinical information from the α- and β-dispersions. Hence, the indexation technique is inappropriate for microinvasive impedance or impedance of skin with damaged SC. Then other numerical tools are preferable, such as Cole-approximation or projection methods (e.g. PCA).

1.2.1.3 Principal component analysis (PCA)

It is easy to measure many variables with modern technique. When measuring many variables (K variables) on a population (N observations) the data can be arranged into a multivariate matrix, **X**, with the size NxK, i.e. N points in a K-dimensional space, or K points in an N-dimensional space. In the impedance case, a number of impedance spectra, N, measured in a frequency range, K frequencies, can be arranged in a multivariate impedance data matrix.

For a multivariate data set it is most likely that the variables are, more or less, correlated, i.e. the variables are not necessarily independent. PCA is used to reduce the number of variables of multivariate data, to compress **X**, and to extract information from **X** using projections. A projection from 3D to 2D is exemplified in figure 15.

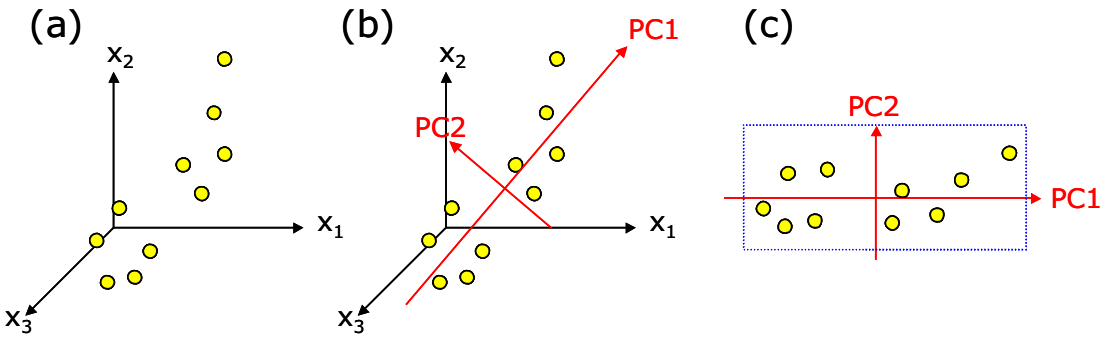

Figure 15. (a). A 3D scatter plot of the variables x1, x2, and x3 measured for a number of observations. (b) Two directions, marked PC1 and PC2, are found that describe most of the variance of the data. (c) Scatter plot of the projected observations from a 3D space to a 2D area.

The main aim of PCA is to reduce dimensionality with a minimum loss of information. The idea behind the PCA is that data can be described as a structural part and a residual part that contain noise. PCA finds directions, principal components (PCs), that describe the structure, the main features of **X**. Each PC consists of a set of scores ($\mathbf{t}_a$) and loadings ($\mathbf{p}_a$). The PCA decomposition is formally given by:

$$\mathbf{X} = \mathbf{1}\bar{\mathbf{x}} + \sum_{a=1}^{A} \mathbf{t}_a \mathbf{p}_a' + \mathbf{E} = \mathbf{1}\bar{\mathbf{x}} + \mathbf{T}\mathbf{P}' + \mathbf{E} \quad ,$$

where **T** (NxA) is the score matrix ($[\mathbf{t}_1, \mathbf{t}_2, \ldots, \mathbf{t}_A]$), $\bar{\mathbf{x}}$ a vector of mean values of the variables of **X**, **P** (KxA) the loading matrix ($[\mathbf{p}_1, \mathbf{p}_2, \ldots, \mathbf{p}_A]$), and **E** (NxK) the residual matrix. The solution to the equation above is found in a least squares manner using the non-linear iterative partial least squares (NIPALS) algorithm [66]. A PCA model is graphically shown in figure 16.

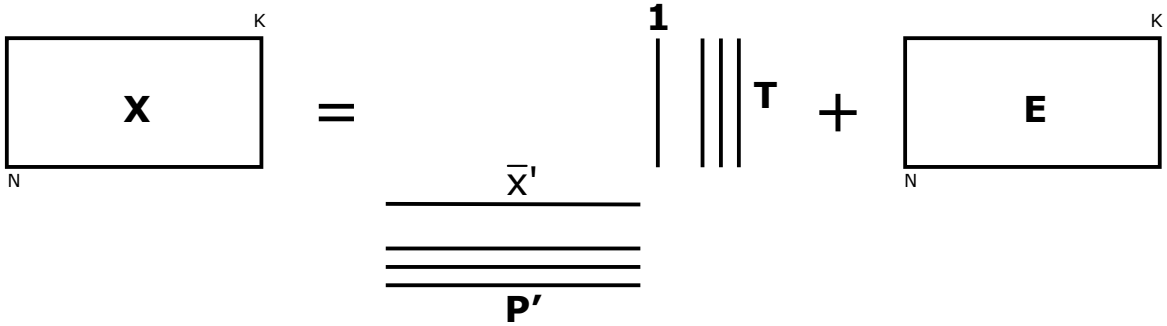

Figure 16. Schematic picture of PCA, i.e. decomposition of the data, **X**, to a structural part, the principal components, and a residual matrix, **E**. Each principal component consists of a set of scores ($\mathbf{t}_i$) and loadings ($\mathbf{p}_i$) that describe how the observations and variables relate to each other.

The number of PCs, A, must be less than or equal to the smallest dimension of **X**, i.e. $A \leq \min\{N,K\}$. The PCs are said to be orthogonal, i.e. they are independent of each other. The PCs are size ordered according to the explained variance of **X**; the first PC describes the largest part of the variance of **X**.

The scores describe how the objects relate to each other, and the loadings how the variables relate to each other. Analysing the scores makes it is possible to find trends and outliers. Analysing the loadings gives information of how the variables correlate to each other, and which variables are significant and which are unimportant for the model.

The idea of projecting multivariate data to subspaces was first published in 1901 [67] and the PCA technique is described in detail in [66, 68-70]. PCA was used to simplify electrical impedance data in e.g. [71-73], to simplify electrical skin impedance in [32, 74], and to simplify electrical impedance spectra of skin lesions in [52, 57].

1.2.1.4 Parallel factor analysis (PARAFAC)

Some techniques and instruments generate a data matrix for each measurement, for example fluorescence excitation-emission measurements, and impedance spectra measured in a frequency interval at several depth settings. The data of such techniques can be arranged in multi-way arrays, **X** (figure 17). In the impedance case, the corresponding structure of the array would be subjects x depth settings x frequencies, i.e. a three-way data set

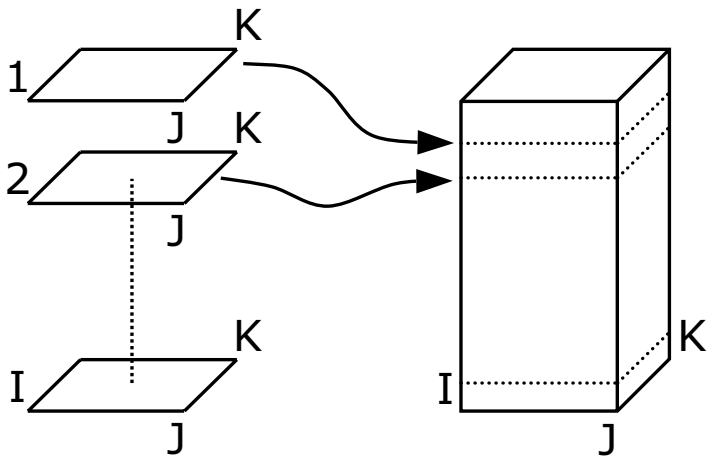

Figure 17. Arranging several matrices into a three-way data array **X** (IxJxK).

with three modes.

The main idea behind PARAFAC is to simplify multi-way data to a structural part and a residual part using linear projections. Parallel factor analysis can be used to find directions, PARAFAC components, that describe the underlying pattern of the data, to decompose **X** into sets of loadings that describe the systematic variations of the data. Using PARAFAC, the data is reduced to a set of loading vectors, one vector for each mode and PARAFAC component, visualised in figure 18. Formally, each data point x_{ijk} of **X** is given by:

$$x_{ijk} = \sum_{r=1}^{R} a_{ir} b_{jr} c_{kr} + e_{ijk} ,$$

where a_{ir}, b_{jr}, and c_{kr} are typical elements of the loading vectors $\mathbf{a}_r$, $\mathbf{b}_r$, and $\mathbf{c}_r$ of mode A, B, and C, respectively. R is the number of PARAFAC components, and e_{ijk} is an element of the residual array **E**.

The PARAFAC loadings describe how the variables in each mode relate to each other, and also how they relate to the other modes. Hence, the PARAFAC loadings can, to some extent, be interpreted in a similar manner as the PCA components.

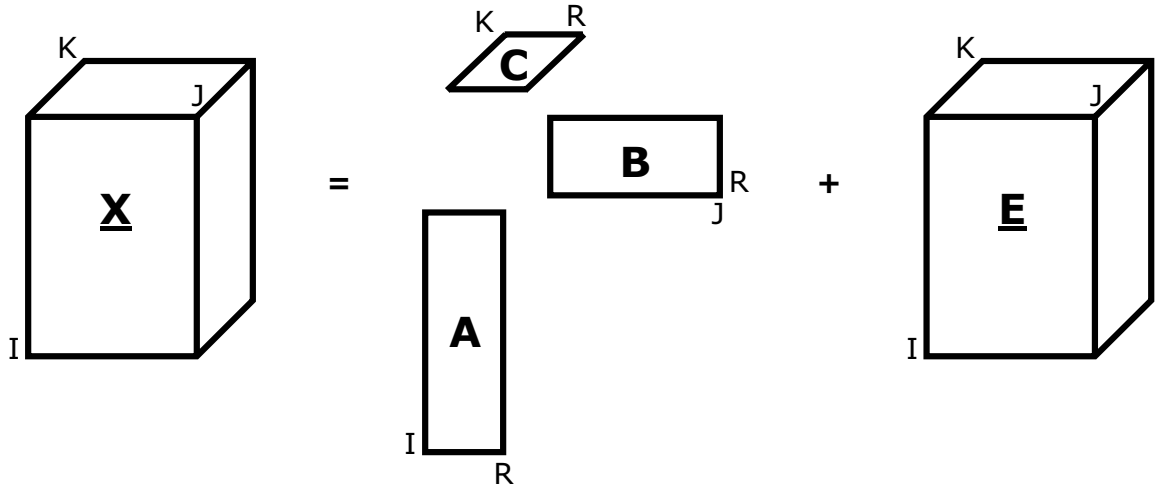

Figure 18. Schematic visualisation of PARAFAC decomposition of a three-way array **X** (IxJxK). **E** is the residual array. R is the number of PARAFAC components, and **A**, **B** and **C** are the loading matrices of the first, second and third mode, respectively.

The PARAFAC algorithm provides unique solutions for real multi-way data with acceptable signal-to-noise ratio. If the appropriate number of PARAFAC components is used, the loadings represent the true underlying pattern, i.e. PARAFAC can be used as a curve resolution tool. For example, PARAFAC decomposition of fluorescence excitation-emission measurements gives pure spectra of the excitation and emission spectra of the fluorophores in the measured samples [75, 76].

The most general multi-way models are Tucker models [77], proposed by the psychometrican Tucker in 1966 [78]. It is a generalization from two-way PCA to multi-way decomposition. The Tucker algorithm decompose a three-way **X** (IxJxK) to three sets of loading matrices, **A** (IxP), **B** (JxQ), and **C** (KxR), for modes A, B, and C, respectively, a core array **G** (PxQxR), and a residual array, **E** (IxJxK), according to:

$$x_{ijk} = \sum_{p=1}^{P} \sum_{q=1}^{Q} \sum_{r=1}^{R} a_{ip} b_{jq} c_{kr} g_{pqr} + e_{ijk} .$$

a_{ip}, b_{jq}, and c_{kr} are typical elements of the Tucker loadings matrices; and g_{pqr} is a typical element of **G**. There can be different number of components for each mode, e.g. P, Q, and R components, for mode A, B, and C.

The core array describes the interaction between individual loadings of different modes. The PARAFAC model is a constrained Tucker model, or a special case of Tucker. In PARAFAC, the diagonal elements of the core array are equal to one and the non-diagonal elements are equal to zero. Core consistency is a tool for finding the right number of PARAFAC components. The core consistency is a quality measure of how well a PARAFAC solution represents the variation in the data consistent with the core constraints. Ideally, the core consistency is 100%, which mean that the PARAFAC loadings give an appropriate description of **X**. A core consistency distant from 100% is an indication that a PARAFAC model with fewer components will provide a better solution. The core consistency diagnostics is described in detail in [79].

PARAFAC decomposition was proposed simultaneously and independently by Harshman [80] and Carrol and Chang [81] in 1970, and is described and exemplified in [82-85]. Bro et al. [86] made a PARAFAC algorithm for complex valued three-way arrays, which might be useful for complex skin impedance spectra. PARAFAC decomposition of skin impedance is described in paper **I**.

1.2.2 Classification techniques

The aim of numerical classification of electrical impedance and skin cancer is to find rules that describe the relationship between impedance spectra and lesion type. The overall motivation is to use the classification rules to identify the group membership of new anonymous lesions using impedance measurements. In order to do so, the numerical classifier has to be trained, i.e. the rules have to be adjusted for the specific problem using a training set, i.e. impedance measurements of lesions with known group membership.

It is important to evaluate the performance of the classifiers, to validate the classification models. Validation can be done in different ways, e.g. using measurements of new lesions, and cross-validation. Measurement of new lesions with known group membership, i.e. a test set, after the rules have been determined is the most reliable and fair way of validation, a procedure which mimics the intended use of the classifier. However, diagnosis of new lesions with the gold standard can be expensive in terms of time, money, and effort. In such case, the training set itself can be used as test set in cross-validation to approximate the performance. It is an iterative process where the test set is randomly split in a number of subsets. For each iteration, one subset is left out of the training set, the remaining observations are used to model the classification, and finally the model is used to predict the class membership of the excluded subset. The process is repeated until all subsets have been used as test set once. The performance of the classification is then approximated using the relation between observed and predicted group membership of the subsets. If the number of subsets is equal to the total number of samples in the training set, the validation is called leave-one-out cross-validation. Cross-validation can also be used to determine the complexity of classification models.

Various classification techniques have been used to analyse impedance data, however this thesis focuses on a limited selection that have been used in papers **II**, **III**, and **V**, and in [57] to separate impedance measurements of benign nevi and skin cancers: linear discriminant analysis (LDA), soft independent modelling of class analogy (SIMCA), and receiver operating characteristics (ROC). Both LDA and SIMCA are based on projections. The LDA technique focuses on dissimilarities between groups of data, whereas SIMCA classification focuses the similarities within classes. ROC technique is simple classification of univariate data, and hence not very appropriate for multivariate problems. However, the ROC technique is useful in evaluating the performance of more advanced classification techniques, such as the outcomes of LDA and SIMCA classifications.

1.2.2.1 Receiver operating characteristics (ROC)

Suppose that we have measured a continuous variable in a population and we want to correlate this variable to a feature, i.e. to classify the population. According to a gold standard, some of the subjects have the feature, e.g. skin cancer, and the others do not, e.g. benign lesions. A subject with the feature is called positive, and a subject without negative. At a certain threshold, or a difference limit, a subject can be judged correct or incorrect, i.e. a true or false classification based on the measured variable. When separating overlapping groups a degree of misjudging is inevitable, and hence it is important to describe the performance of the classification, e.g. in terms of sensitivity and specificity. Sensitivity is the ability to single out those subjects with the feature tested for. For example, if the sensitivity equals 100% it means that all subjects in a population with the feature are detected. That is obviously a desired property of a method, but the sensitivity does not say anything about the number of misjudged negative subjects. The specificity, however, is the ability to identify those subjects without the feature. In terms of skin cancer detection, sensitivity is the probability that a malignant lesion will give a positive impedance test result, and specificity the probability that a harmless lesion will give a negative impedance test result, given by:

$$\text{sensitivity} = TP/(TP+FN)$$
$$\text{specificity} = TN/(TN+FP)$$

TP (true positive) is the number of skin cancers with positive impedance test result, TN (true negative) the number harmless lesions with negative impedance test result, FP (false positive) the number harmless lesions with positive impedance test result, and FN (false negative) is the number of skin cancers with negative impedance test result, shown in figure 19. Other parameters used to describe the performance of a medical diagnostic tests are the positive (PPV) and negative predictive values (NPV), given by:

$$PPV = TP/(TP+FP)$$
$$NPV = TN/(TN+FN)$$

PPV is the probability that a lesion really is malignant given a positive impedance test result, and the NPV is the probability that a lesion is harmless given a negative impedance test result. The PPV and NPV depend on the prevalence of the disease, which implies that these parameters are useful when the test subjects are chosen randomly from the population. Interpretation of PPV and NPV is ambiguous if the test subjects in the study do not represent the overall population, i.e. PPV and NPV of a skin cancer screening technique is useful if the ratio between number of cancers and the number of benign lesions represent the true relation between skin cancer and benign lesions in the population that undergo screening. Sensitivity and

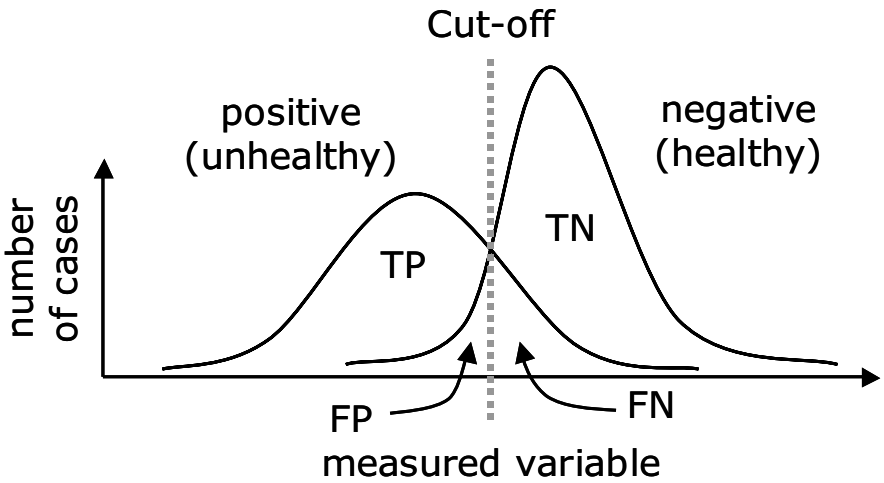

Figure 19. Histogram of a measured variable of two groups (e.g. healthy and unhealthy) diagnosed using a gold standard method. The cut-off corresponds to the level where the subjects are classified positive or negative. If the two groups are overlapping, there will be a degree of misjudging. Thus, classification of a positive subject can be true positive (TP) or false negative (FN), and classification of a negative subject can be true negative (TN) or false positive (FP).

specificity do not depend on the prevalence.

If the threshold in figure 19 is moved iteratively from minimal to maximal value of the measured variable, the sensitivity will increase from 0% to 100%, whereas the specificity will decrease from 100% to 0%. A plot of (1 – specificity) on the x-axis and sensitivity on the y-axis of the iterations is called a receiver operating characteristic (ROC) curve. ROC curves are used to judge the discriminative ability of various statistical methods and test results for predictive purposes [87]. The area under the ROC curve (AUC) is an estimate of the probability that a randomly chosen subject is correctly diagnosed, i.e. the AUC is a representation of the overall diagnostic accuracy of the technique, described in [88-90]. Random guessing would result in an AUC of 0.5. If AUC is 1.0, the diagnostic accuracy of the test is ideal, which means that there is perfect separation between the groups, and sensitivity and specificity are close to 100%. The ROC analysis is a non-parametric tool. Hence, there are no distribution constraints, e.g. the data does not have to have Gaussian distribution. The standard error, SE, of the AUC is given by [88]:

$$SE=\sqrt{\frac{AUC(1-AUC)+(n_A-1)(Q_1-AUC^2)+(n_N-1)(Q_2-AUC^2)}{n_A n_N}},$$

where n_N and n_A are the number of normal and abnormal subjects, respectively. Q_1 and Q_2 are given by: $Q_1=AUC/(2-AUC)$, and $Q_2=2AUC^2/(1+AUC)$. Generally, the SE decreases with increasing AUC, e.g. the error is higher when the groups are overlapping than when there is a clear separation between the groups.

The ROC curve are remarkably useful tools in medical decision-making, and electrical impedance was used together with ROC e.g. in cervix cancer detection [91], in detection of malignancy areas in the bladder [92], and to describe the performance of separation of malignant and benign cutaneous lesions in [55, 56].

1.2.2.2 Linear discriminant analysis (LDA)

A measured set of data $\mathbf{X}$, with individual measurements $\mathbf{x}_i$, that corresponds to a specific binary feature $\mathbf{y}$, e.g. malign or benign tissue, can be used to calibrate a numerical classifier. The classifier can then, if the model is accurate, be used to identify the group membership of unknown samples. Fisher's linear discriminant analysis is a simple classifier that is based on linear projections of the variables of $\mathbf{X}$ onto a discrimination direction, $\mathbf{w}$. The LDA technique was developed by Fisher in 1936, and is described in [93-96]. A brief summary is given in this section. The objective of LDA is to find an equation, $f(\mathbf{x}) = \mathbf{w}'\mathbf{x} + b$, that projects the samples, $\mathbf{x}_i$, linearly onto the discriminant direction, $\mathbf{w}$, that separates the mean values, μ_k, of the two classes, k, while achieving a small variance around these class means, σ_k, Thus the projection maximises the between-class variation and minimises the within-class variation, as shown in figure 20. The discriminant direction is given by $\mathbf{w} = \mathbf{S}_W^{-1}\left(\bar{\mathbf{x}}_1 - \bar{\mathbf{x}}_2\right)$. $\mathbf{S}_W^{-1}$ is the within-class-covariance matrix, and $\bar{\mathbf{x}}_k$ the mean vector of class k, according to:

$$\bar{\mathbf{x}}_k = \frac{1}{n_k}\sum_{i=1}^{n_k}\mathbf{x}_i^{(k)} \quad \text{and} \quad \mathbf{S}_W = \frac{1}{n}\sum_{k=1}^{K}\sum_{i=1}^{n_k}\left(\mathbf{x}_i^{(k)} - \bar{\mathbf{x}}_k\right)'\left(\mathbf{x}_i^{(k)} - \bar{\mathbf{x}}_k\right),$$

where n_k is the number of samples in class k, and $\mathbf{x}_i^{(k)}$ is the i:th sample of class k. The bias of the discriminant equation, b, is calculated according to $b = -0.5 \cdot \left(\mathbf{w}'\bar{\mathbf{x}}_1 + \mathbf{w}'\bar{\mathbf{x}}_2\right)$. Classification of an unknown sample $\mathbf{x}_i$ is based on the outcome of the discriminant equation: if $f(\mathbf{x}_i)$ is larger than or equal to zero, the unknown sample belongs to class 1, and if $f(\mathbf{x}_i)$ is smaller than zero, $\mathbf{x}_i$ belongs to class 2. In the skin cancer and electrical impedance

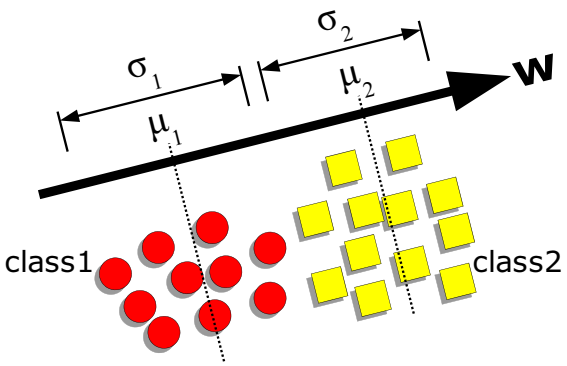

Figure 20. The Fisher's discriminant direction **w** maximises separation of the groups, $(\mu_1-\mu_2)^2$, and minimises the within groups variations, $(\sigma_1+\sigma_2)$.

context, the classification rule might look like:

$$y = \begin{cases} \text{"benign" if } f\left(\mathbf{z}=|\mathrm{Z}|\mathrm{e}^{\mathrm{i}\theta}\right) \geq 0 \\ \text{"cancer" if } f\left(\mathbf{z}=|\mathrm{Z}|\mathrm{e}^{\mathrm{i}\theta}\right) < 0 \end{cases}$$

The linear discriminant approach is applicable when there is an inverse to the within-class-covariance matrix, when $\mathbf{S}_W^{-1}$ exists. For highly multivariate and collinear data, e.g. electrical impedance spectra, the $\mathbf{S}_W^{-1}$ can be unstable, or singular if the number of variables exceed the number of observations, and thus LDA cannot be used for ill-conditioned data. Reducing the dimensions of the data, e.g. with PCA, prior to LDA classification is a reasonable approach for multivariate data. The scores of the PCA model can then be used to find the $\mathbf{S}_W^{-1}$, described in [97].

Fisher linear discrimination analysis is one of the simplest forms of classification techniques, and it is appropriate when the classes are linearly separable (figure 21a). However, this is seldom the case for real life measurements, and especially not for skin cancer assessments where e.g. a benign lesion can progress gradually to malignancy and the classes are overlapping. Linear discrimination is useless for asymmetric data where e.g. classes are embedded (figure 21b), or for other highly complex data structures, such as the example in figure 21c. Then, other classification tools are preferable, such as soft independent modelling of class analogy, k-nearest neighbours, and artificial neural networks, which can handle non-linearities, discussed in [98]. Thus, the choice of classification technique is dependent upon the complexity of the data. As a rule of thumb, with

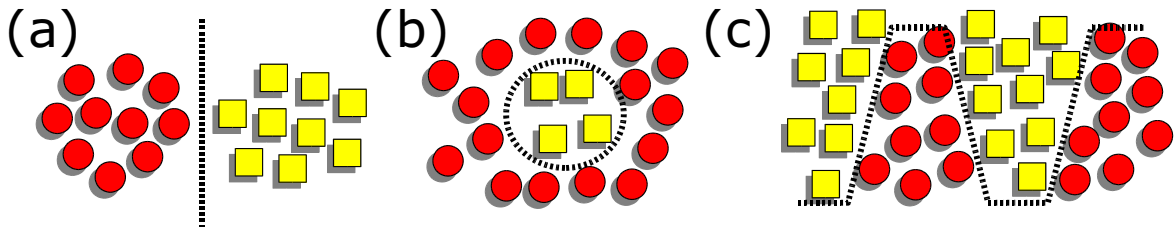

Figure 21. Types of clustering of data from two classes. For the symmetrically distributed data in (a) it is possible to separate the groups without errors using linear discrimination. The groups in the asymmetric data (b), and in the complex data (c) are linearly inseparable, and it is not possible to separate the two groups without errors using linear discrimination.

increasing data complexity, more advanced numerical classifiers are required to avoid misclassifications, and more measurements are needed in the training set to avoid over-fitting of the models. A practical consequence of this rule of thumb is that the choice of numerical classification technique is also dependent upon the number of subjects available in the training set, or the total number of samples if cross-validation is used.

1.2.2.3 Soft independent modelling of class analogy (SIMCA)

Soft independent modelling of class analogy is a supervised classification technique that is based on a set of PCA models, one PCA_k model for each class k. The PCA_k models capture the main features of a training data set, $\mathbf{X}_k$, of each corresponding class and define limits around the classes. It is possible to use different number of principal components for each PCA_k model, which makes SIMCA a flexible and versatile pattern recognition tool. In order to determine the group membership of an unknown measurement, $\mathbf{x}_i$, the sample is fitted to the PCA_k models, and the distances, d_k, between the unknown sample and the classes, as shown in figure 22, are used to classify the reading. The classification rule is: the sample belongs to the class closest to $\mathbf{x}_i$, i.e. the unknown sample belongs to the class with minimal d_k. The distances are approximated from the scores and the residuals of the PCA_k models. The SIMCA model is described in e.g.

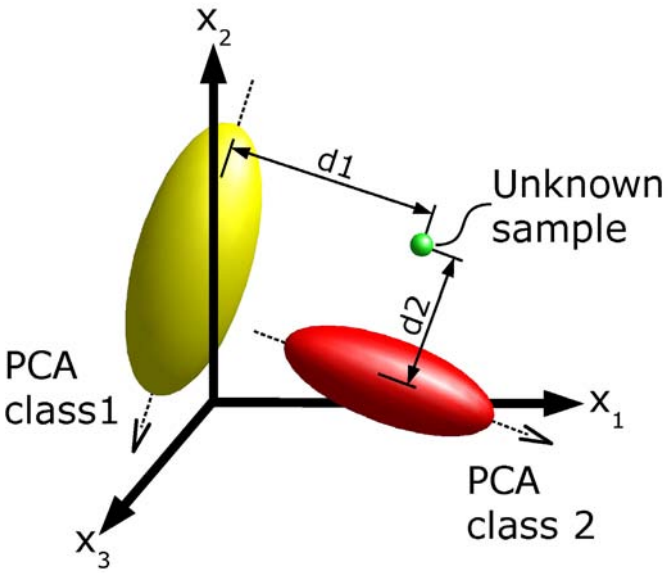

Figure 22. Simplified schematic figure of SIMCA classification of an unknown sample. The sample is exposed to the individual PCA models, and the unknown sample is predicted to belong to the class with PCA model closest to the sample.

[70, 99, 100].

Formally written, a separate PCA_k model is calculated for the data, $\mathbf{X}_k$, in each class, k, $\mathbf{X}_k = \mathbf{t}_{k1}\mathbf{p}'_{k1} + \mathbf{t}_{k2}\mathbf{p}'_{k2} + \ldots + \mathbf{t}_{kA}\mathbf{p}'_{kA} + \mathbf{E}_k$. Then, the new anonymous sample, $\mathbf{x}_i$, scaled the same way as the training set, is fitted to each separate PCA_k model $\mathbf{x}_i = \hat{\mathbf{t}}_{k1i}\mathbf{p}'_{k1} + \hat{\mathbf{t}}_{k2i}\mathbf{p}'_{k2} + \ldots + \hat{\mathbf{t}}_{kAi}\mathbf{p}'_{kA} + \mathbf{e}_{ki}$. Scores of the unknown samples, $\mathbf{t}_{ki}$, are approximated, and the residuals, $\mathbf{e}_{ik}$, are calculated for each class, according to: $\mathbf{t}_{ki} = \mathbf{x}_i\mathbf{p}'_k$, $\mathbf{e}_{ki} = \mathbf{x}_i - \hat{\mathbf{t}}_{ki}\mathbf{p}'_k$. For each sample, the distance to the models is calculated from the residuals, Q, and the scores, called Hotelling's T^2, shown in figure 23. The Q_i for the unknown sample $\mathbf{x}_i$ represents the lack of fit to the model, and is simply the sum of squares of the residuals, $Q_i = \sum \mathbf{e}_i^2$. The Hotelling's T^2 statistic is a measure of the variation in each sample within each PCA_k model, a measure of the distance to the centre of the model. It is calculated from the scores of the unknown sample, $\hat{\mathbf{t}}_{ia}$, and the variation, s^2, of the scores of the training set, $\mathbf{t}_{ia}$, for every component according to: $T_i^2 = \sum \hat{\mathbf{t}}_{ia}^2 / s_{t_a}^2$. Confidence limits of the Hotelling's T^2 and the Q-residuals, $T^2_{k95\%}$ and $Q_{k95\%}$, can be established for each individual PCA model (figure 23), which represent the normal range of samples within the actual models. The confidence limits are used to normalise the T^2 and Q of the sample, according to: $T^2\text{red}_{ki} = T_{ki}^2 / T_{k95\%}^2$, and $\text{Qred}_{ki} = Q_{ki} / Q_{k95\%}$, and the normalised T^2 and Q provide an estimate of the distance of the unknown sample from each class, according to: $d_{ki} = [(T^2\text{red}_{ki})^2 + (\text{Qred}_{ki})^2]^{0.5}$. The unknown sample is predicted to

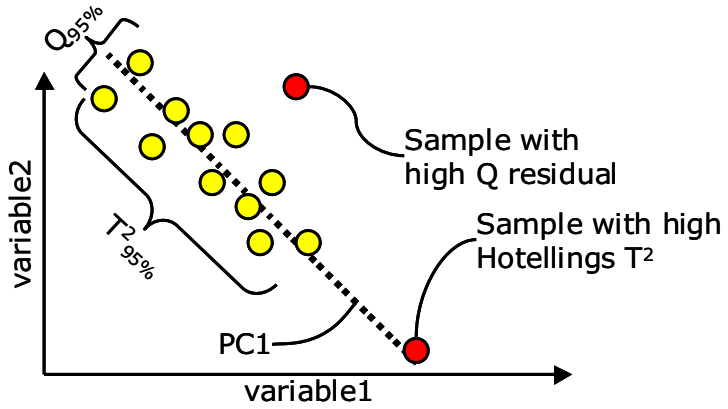

Figure 23. Exemplification of Q and Hotelling's T^2 in a one-component PCA model of a bivariate data set: a sample with unusual variation outside the model, i.e. large Q residual, and a sample with unusual variation within the PCA model, i.e. large T^2. The 95% confidence intervals of the Q-residuals and the Hotelling's T^2, $Q_{95\%}$ and $T^2_{95\%}$, is the range where samples are located with 95% probability.

belong to the closest class.

There are different ways to construct the classification criteria in SIMCA models, demonstrated in [101]. The procedure described above is implemented in the PLS Toolbox software for MATLAB [102], and was used in [57] to separate electrical impedance of BCC and benign nevi.

2 AIMS OF THE STUDIES

THE overall aim of this work is to distinguish harmful from harmless skin lesions, i.e. to separate benign nevi from various skin cancer types and potentially harmful lesions using multi-frequency electrical impedance technique. Specific aims of the individual studies are:

I to describe the impedance variations within volar forearms of normal skin of healthy volunteers, i.e. to investigate the baseline impedance variations within a small area of volar forearms

II to compare lesion and reference impedance

III to evaluate the accuracy of the non-invasive impedance technique to distinguish NMSC and MM from benign nevi

IV to describe the novel microinvasive technique and to exemplify with non-invasive and microinvasive skin impedance measurements

V to compare the accuracy of the non-invasive and microinvasive impedance techniques to distinguish skin cancer from benign nevi

3 MATERIALS AND METHODS

THE depth resolved SciBase impedance spectrometer [SciBase AB, Huddinge, Sweden] was used in all experiments. The outcome of the instrument is magnitude (Ohm) and phase (deg) from 5 levels of depth penetration at 31 logarithmically distributed frequencies from 1 kHz to 1 MHz. The impedance spectrometer is connected to a laptop and a probe. The operator controls the instrument via the laptop and the laptop records all impedance spectra. The instrument set-up is shown in figure 24. The multi-frequency depth resolved impedance technique is described in [34].

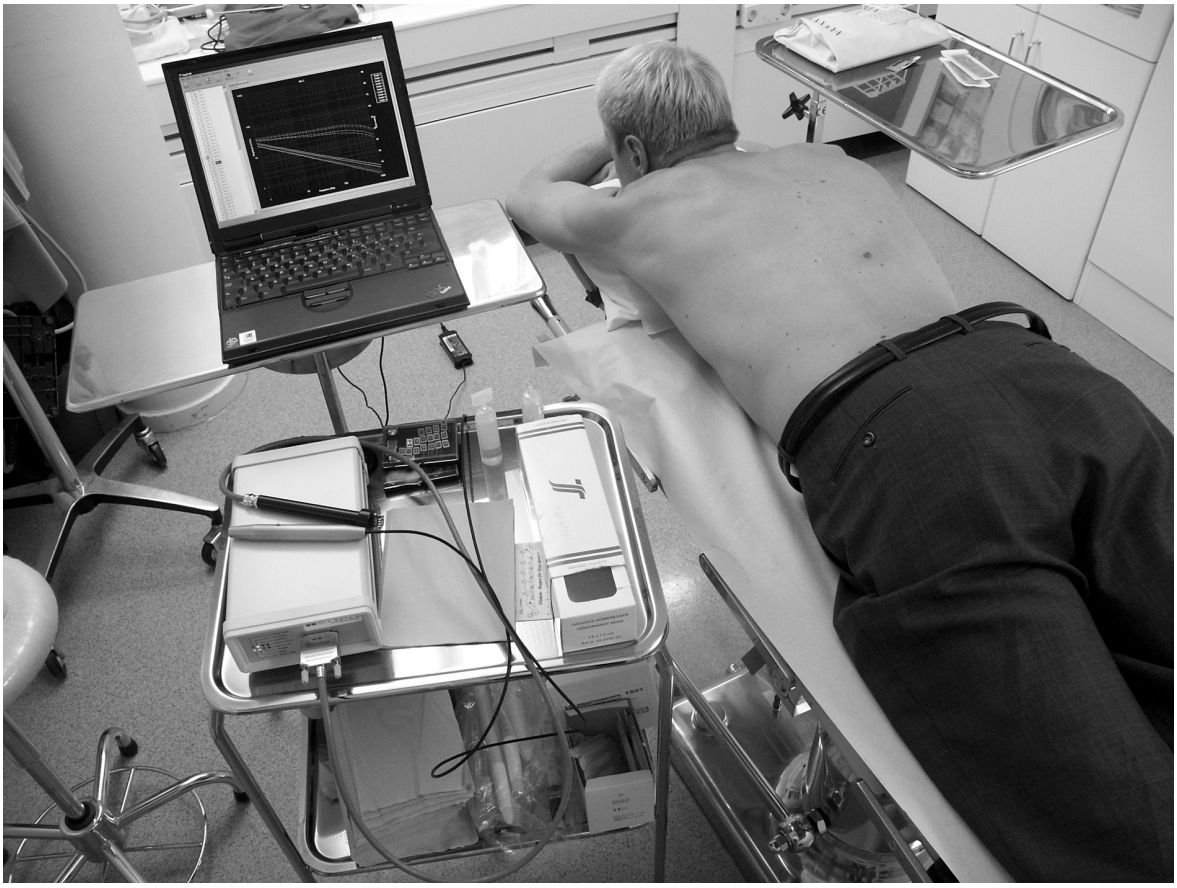

Figure 24. Instrument set-up at the department of Surgery, Läkarmottagningen Hötorget, Stockholm, Sweden: the SciBase II impedance spectrometer with the microinvasive and non-invasive skin probes on the top, a laptop, and a volunteer with a suspect lesion on the back.

Figure 25. The SciBase I (left) and II (right) depth resolved impedance spectrometers used in the studies.

There are two versions of the spectrometer, SB I and II (figure 25). The difference between the instruments is their detectors. In SB I there are two detectors; one is measuring magnitude, and the other phase angle, and in SB II there is just one detector. The SB II detector measures both the resistance and reactance, one at a time. Then the instrument converts the complex impedance to polar coordinates and the output is magnitude and phase. The main difference between the two instrument versions is the degree of immunity to external electromagnetic interference, and impedance spectra measured with SB I can, if the electromagnetic noise levels in the surroundings are high, be degraded, while SB II is virtually immune to external noise sources.

All lesion measurements were made at the department of Surgery, Läkarmottagningen Hötorget, Stockholm, Sweden. The patients included in the studies came to the clinic after self-examination or by refferal from other physicians. At the clinic, an experienced surgeon screened the patients for skin cancer. Measurements of suspicious lesions were made with an electrical impedance spectrometer over the centre of the lesion, and an ipsi-lateral reference skin site was measured for each lesion. The suspect lesions were located at various body sites, with some lesion types preferentially in the head/neck and shoulder regions, which are more exposed to sun radiation. Before the measurements, the reference skin and lesions were soaked with 0.9% physiological saline solution (pH 6) for approximately one minute to reduce the naturally high impedance of the stratum corneum and to increase the contact between the probe and tissue. An impedance measurement takes approximately 20 seconds. After the measurements, the lesions were excised and diagnosed by histology. The lesions in the studies

were 4 mm in diameter or larger. The same histopathologist diagnosed all lesions. Subclassifications of the lesion types have not been considered. The same operator was used throughout the studies. Huddinge University Hospital Ethical Committee for Human Research, Huddinge, Sweden, approved the electrical impedance measurements of lesions.

In paper **I**, non-invasive skin impedance spectra and trans epidermal water loss (TEWL) were measured on 27 healthy volunteers (12 females and 15 males) between 18 and 30 years of age at different locations on the volar forearms. The sites were oriented in a specific pattern, according to figure 26. The directions sx, sy, and sz describe the locations in terms of outer or inner side of the arm (sx), upper or lower side of the arm (sy), and left or right arm (sz).

TEWL is a value of the passive diffusion of water through the stratum corneum [103, 104]. The outcome of the Evaporimeter instrument is water mass per area and hour (g m^{-2} h^{-1}). The TEWL was measured using the Evaporimeter EP1 [Servomed, Kinna, Sweden], and the SB II impedance spectrometer was used to measure the electrical impedance.

TEWL and MIX of the three directions were investigated using three-way ANOVA in the SPSS 11.0 software [SPSS Inc., Chicago, IL, USA]. Full impedance spectra were simplified to two PARAFAC components using the PLS-toolbox for MATLAB [102], and the N-way toolbox for MATLAB [105].

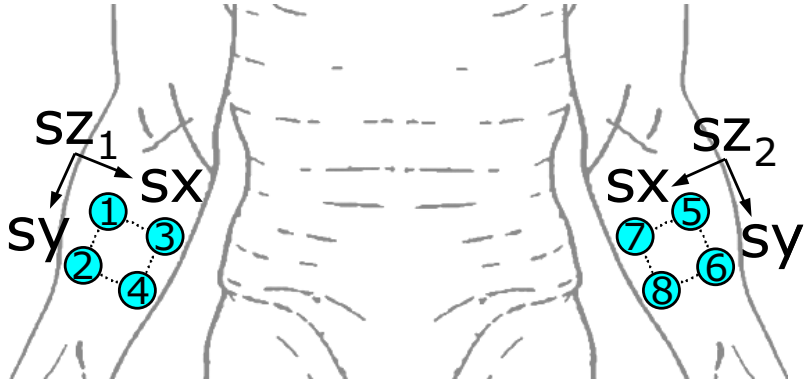

Figure 26. The eight sites used in the experiment were chosen to cover outer and inner sides of the arms (sx), upper and lower sides (sy) at both arms (sz). The sites were placed 4-5 cm apart.

In paper **II**, non-invasive impedance spectra of 258 benign pigmented nevi, 34 BCC, 17 dermatofibromas, 35 dysplastic nevi, and 26 seborrheic keratoses were measured using the SB I instrument. The differences between the lesions and their controls with respect to the four impedance indices were investigated using the Wilcoxon Signed Ranks Test for independent samples in the SPSS 11.0 software [SPSS Inc., Chicago, IL, USA].

In paper **III**, non-invasive impedance spectra of 511 benign pigmented nevi, 94 NMSC and precancerous lesions (i.e. 79 BCC, 6 SCC, and 9 actinic keratoses), and 16 MM were measured using the SB II instrument. The impedance spectra were parameterized using squared correlation coefficients, r^2, of the linear relation between lesion and reference impedance. Simple linear cut-offs of the r^2-parameters were used to distinguish the harmless nevi and the skin cancers.

In paper **IV**, non-invasive and microinvasive impedance spectra of healthy skin, an actinic keratosis, and a dysplastic nevus were measured using the SB II instrument.

In paper **V**, non-invasive and microinvasive impedance spectra of 99 benign pigmented nevi, 28 BCC, and 13 MM were measured using the SB II instrument. The impedance spectra were parameterized using both PCA and the r^2-parameters derived in paper **III**. Classification of the lesions was made using LDA, and the sensitivities and specificities of the techniques were estimated using cross-validation. PCA models were calculated using the PLS toolbox for MATLAB [102], and the Statistics Toolbox for MATLAB [MathWorks, Natick, Massachusetts, USA] was used to calculate the LDA models.

4 RESULTS AND DISCUSSION

4.1 PAPER I

THREE-way ANOVAs of TEWL and MIX showed that there was a significant difference between the outer and inner sites of the volar forearms (TEWL $p<0.01$, and MIX $p<0.001$), whereas PARAFAC of the full impedance spectra showed that there were substantial differences both for the outer vs. inner sides of the arms (figure 27a), as well as between right and left arms (figure 27c).

Paper **I** demonstrates, in line with previous investigations [28, 106-110], that the baseline of human skin properties varies with body site. It is not clear why no difference between left and right arms was found for TEWL even though it has been reported in the literature that such differences exist [107]. Maybe it is an effect of the limited number of sites used. Nevertheless, differences between right and left arms were found for the impedance. This indicates that the impedance technique is more precise than TEWL, at least in this example. The advantage of electrical impedance over TEWL has previously been shown for several applications [34].

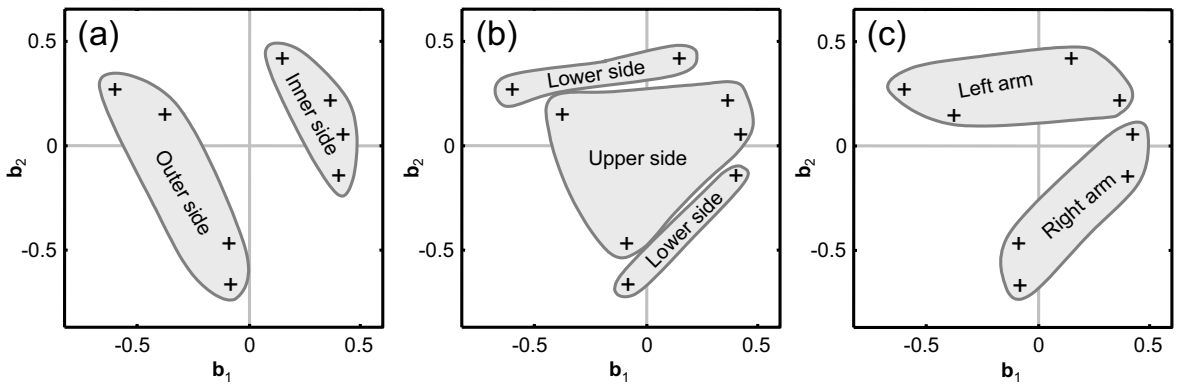

Figure 27. Scatter plot of the two PARAFAC components ($\mathbf{b}_1$ vs. $\mathbf{b}_2$) describing the sites. The sites are marked with +. The three figures show the same components with different regions marked: (a) sites on inner and outer sides of the arms, (b) upper and lower sides of the arms, and (c) the left and right arms.

The measurement order was not randomised, and for the majority of the volunteers the sites were measured in the order the sites are numbered in figure 26. This is a limitation, and sceptics might say that the results in this experiment show measurement variability rather than a body-location variation. This could be true for the TEWL, where it is known that e.g. nervousness and stress affect the readings, and there is a theoretical possibility that these properties varied throughout the experiment. The skin impedance technique is believed to be unaffected by such variations. However, the measurements were made by an experienced operator who calmed the volunteers and let them rest prior to the TEWL readings. Moreover, the TEWL readings did not show any chronological patterns, i.e. the amount water evaporating from the skin did not show any trends over time, which indicates that randomisation was not critical for the TEWL in this study.

Within the relatively local area, such as the volar forearm, which is frequently used in skin research and cosmetological testing, the skin property variations are surprisingly big. This implies that utmost care in the study design must be enforced to facilitate observations of subtle reactions. To prevent the variability of the skin properties of volar forearm from overshadowing the dermal responses in skin testing, proper experimental design must to be used, e.g. randomisation, differential measurements, and repeated measures (replicates), and reference sites should be carefully located contra-laterally or ipsi-laterally – but following the same site in time is obviously optimal. As demonstrated in this work, any ipsi-lateral reference reading on volar forearms should be chosen lengthwise along the arms rather than sideways.

4.2 PAPER II

IMPEDANCE indices of 4 out of 5 lesion types were significantly different from their controls: nevi vs. references ($p<0.001$), BCC vs. references ($p<0.001$), dysplastic nevi vs. references ($p<0.01$), and seborrheic keratosis vs. references ($p<0.01$). There was no significant difference between dermatofibroma and reference skin.

Of course, it is more interesting to classify individual readings rather than identifying statistical differences between lesions and their references. Classification was evaluated using multivariate numerical methods (e.g. PCA, PARAFAC, and PLS), but it was found that the degree of overlapping between the lesion types was too high and the impedance variance within a group was almost as high as between groups using this technical and numerical approach, and hence the accuracy was limited.

Later on, in addition to the statistically significant differences between lesions and references in paper **II**, the diagnostic power of classification of benign nevi, BCC, and references was investigated using ROC analysis of raw impedance spectra (the same data as in paper **II**) in the SPSS 11.0 software. It was found that AUCs of nevi vs. references, BCC vs. references, and nevi vs. BCC were higher than 80%, as demonstrated in figure 28, i.e. the probability of correct classification was significantly higher than random guessing. The ROC analysis of the data clearly indicated that there is clinically relevant information in the impedance spectra that to some degree can be used to distinguish cutaneous lesions. The ROC analysis of the lesions in figure 28 is published in [56].

4.3 PAPER III

IT was possible to separate the non-melanoma skin cancers and actinic keratoses from the benign nevi with 86.9% specificity (444/511) at 100% sensitivity (94/94), as shown in figure 29 (left), and to identify the

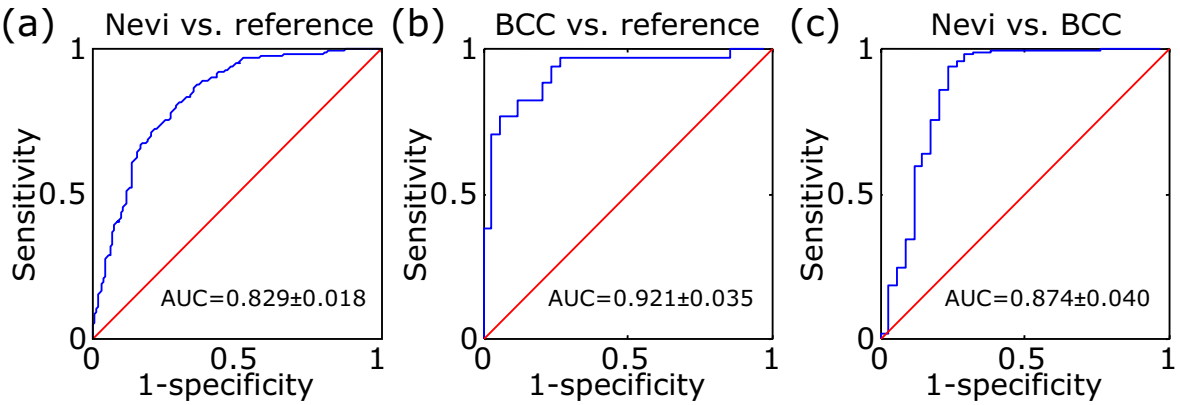

Figure 28. ROC curves of (a) nevi vs. healthy skin, (b) BCC vs. healthy skin, and (c) nevi vs. BCC. Area under curve (AUC) and standard error are marked in the graphs. The diagonal line marks the area where AUC equals 0.5.

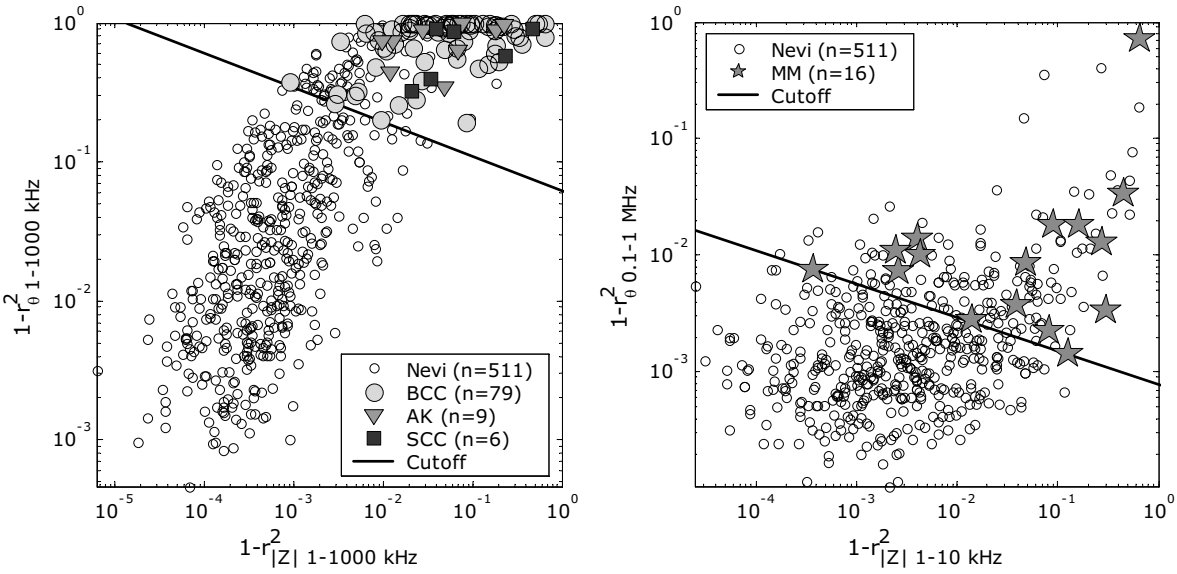

Figure 29. Scatter plots of r^2-parameters of benign nevi, NMSC (left), and MM (right). The cutoff was used to separate skin cancers from the nevi. Measurements above the cutoff were considered to be malignant. The cancer types included in the study are basal cell carcinoma (BCC), squamous cell carcinoma (SCC), actinic keratoses (AK), and malignant melanoma (MM).

melanoma lesions from the nevi with 75.3% specificity (385/511) at 100% sensitivity (16/16), shown in figure 29 (right). ROC area of the NMSCs vs. nevi was 98%, and 89% for MM vs. nevi, shown in figure 30.

These results indicate that the non-invasive multi-frequency electrical bio-impedance technique is a powerful tool in identifying skin cancer, in particular non-melanoma skin cancer, and actinic keratosis. Although we did not use dermoscopy, and the study was not designed to compare the

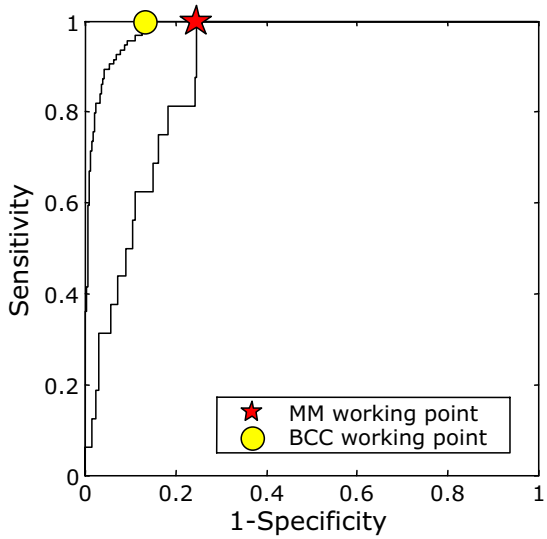

Figure 30. ROC curves of the separation of NMSC and actinic keratosis from benign nevi (98.3% area under ROC curve), and identification of MM from benign nevi (89.0% area under ROC curve). The working points used as cutoff levels in figure 29 are marked.

outcomes of conventional visual screening and impedance lesion detection, the sensitivity and specificity of the impedance technique seem to be as good as, or better than, visual screening made by general practitioners [111, 112], and in the same order as dermoscopy [113].

The outcome of the separation of NMSC and benign nevi is in line with [56], however a much higher accuracy was attained although the same frequency interval and depth settings were used. We believe that the improved accuracy is due to the fact that a different impedance spectrometer, virtually immune to external electromagnetic interference, was used in paper **III**. Moreover, we used more robust numerical methods, and a much larger population (e.g. 511 benign lesions is a significantly larger population than 16) than Dua et al. [52] and achieved similar accuracy, which confirms their results. In the report by Glickman et al. [55] only one frequency (2 kHz), without depth the discrimination, was used to separate melanoma and benign lesions, which might explain their somewhat lower accuracy.

A previously unpublished comparison between the two SB instruments is shown in figure 31. The two instruments were not used on the same sets of patients (SB I: 258 benign nevi vs. 34 BCC, and SB II: 467 benign nevi vs. 72 NMSC). However, the same operator and experimental design was used throughout the two series and hence the two measurement series are

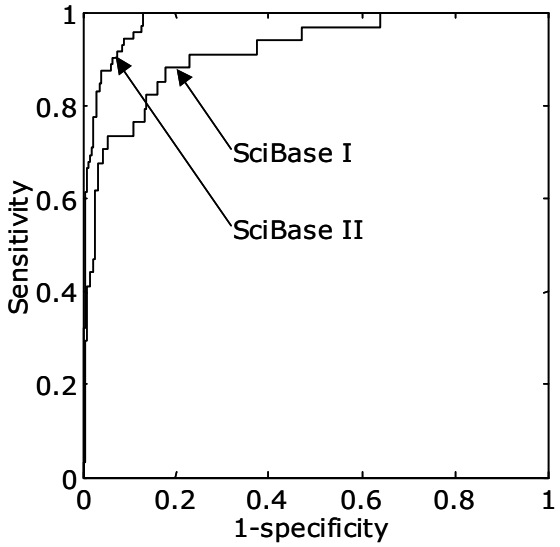

Figure 31. ROC curves of the identification of non-melanoma skin cancer for the SciBase I (lower curve) and SciBase II (upper curve) instruments using the correlation coefficient parameters. Area under ROC curve of the SciBase I instrument was 0.915±0.033, and 0.980±0.012 for the SciBase II instrument.

considered somewhat comparable. Area under ROC curve of the SB I instrument was 0.915±0.033, and 0.980±0.012 for the SB II instrument, indicating that the accuracy of the SB II is, as mentioned above, higher than the SB I version.

From figure 29 it can be concluded that electrical impedance of nevi is more related to reference skin than the cancers. The impedance difference between nevi and NMSC is most likely due to the status of the stratum corneum. The SC of benign nevi is intact, whereas the NMSC is often scaly and occasionally ulcerated, and the barrier function of SC of NMSC is thus degenerated, which easily can be detected with the non-invasive electrical impedance technique, as described in [17]. MM often manifest in the region between the epidermal and dermal layers, and does not affect the SC until the cancer has grown out to the surface of the skin, and the impedance difference between nevi and MM is more sublime because the features of the SC are similar. It is not fully investigated why the impedance of MM differed from nevi, but it is most likely correlated to the structural differences that can be seen histopatologically on the cellular level, e.g. shape, size and orientation differences. Hence, non-invasive impedance of nevi vs. MM is more overlapping than non-invasive impedance of NMSC vs. nevi, and the accuracy is thus higher for the NMSC than the MM lesions.

4.4 PAPER IV

IT was shown that that the influence of the stratum corneum was substantially reduced for skin impedance measured with the microinvasive electrode system compared to skin impedance measured with the regular non-invasive skin impedance probe, as shown in figure 32. The results indicate that the alpha- and beta-dispersions are more discernible for the microinvasive impedance than the non-invasive.

These results indicate that impedance measured with the microinvasive electrode system is fundamentally different from impedance measured with the regular non-invasive probe. The two electrode systems focus on different structures within the multilayers of the skin. Hence, different biological information can be found when using the two probe types: non-

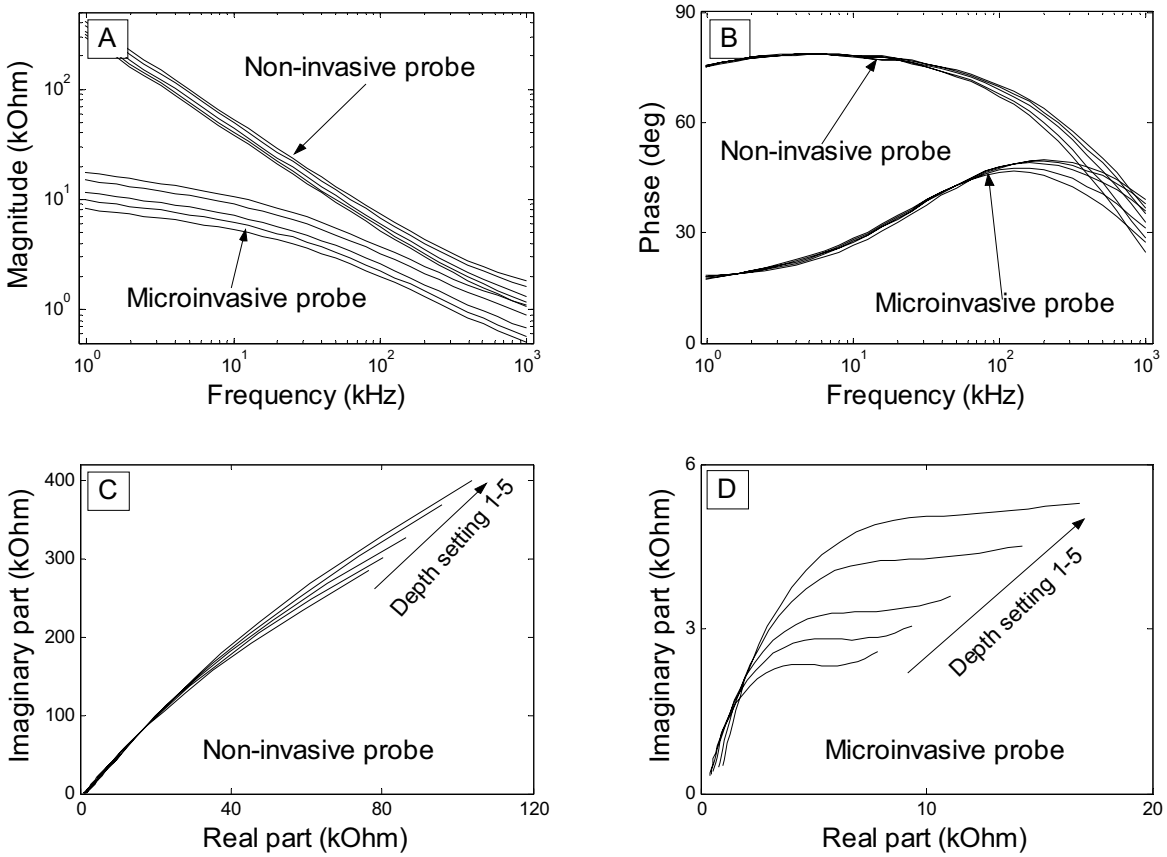

Figure 32. Magnitude and phase spectra at five depth settings of reference skin measured with the microinvasive and the regular non-invasive probes (marked with arrows) (A-B), and the corresponding Nyquist plots of the complex impedance, where the depth settings are indicated with arrows (C-D).

invasive impedance is dominated by the stratum corneum, and microinvasive impedance by the viable skin beneath. The non-invasive probe is therefore preferable when studying the barrier function of the SC, e.g. studies of skin irritations, atopic dermatitis and cosmetological effects, while the microinvasive electrodes seem more appropriate for quantification and classification of the living skin, such as monitoring of allergic reactions, and some skin diseases and in particular MM.

4.5 PAPER V

THE best separation between nevi and BCC was obtained using the regular non-invasive probe (96% sensitivity and 86% specificity), whereas the best separation between nevi and MM was found using the microinvasive electrodes (92% sensitivity and 80% specificity), shown in figure 33. One MM consisted of an atypical nevus with focal transition to MM, thus a somewhat ill defined MM. If this lesion had been excluded the

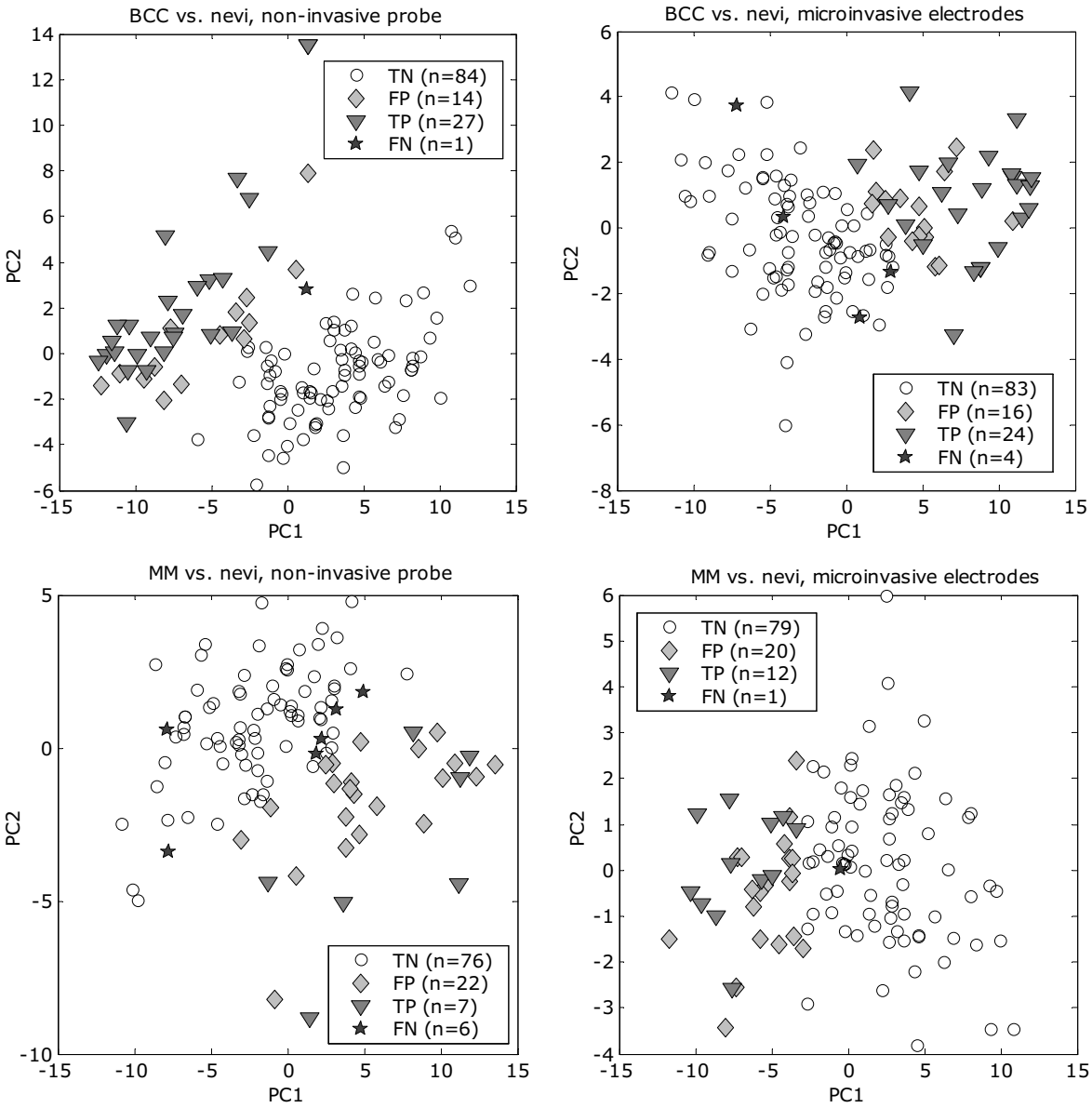

Figure 33. Scatter plots of two PCs of the impedance measured with the regular non-invasive probes (left figures) and spiked microinvasive electrodes (right figures). The lesions are marked according to the outcome of the cross-validated PCA-LDA models (TN = true negative; FP = false positive; TP = true positive; FN = false negative). Separation of BCC vs. benign nevi is shown in the top figures, and MM vs. benign nevi in the bottom figures.

sensitivity would be 100%. Moreover, our results indicate that, for the microinvasive impedance, the PCA simplification seems to be more efficient than the r^2-parameters in distinguishing skin cancer from benign nevi, whereas the accuracy of the two parameterisation methods is approximately in the same order of magnitude for impedance measured non-invasively.

As described in paper **IV**, impedance measured with the non-invasive probe is dominated by the barrier function of the highly impedic stratum corneum.

BCCs are superficial and affect the stratum corneum, whereas MM often manifest in the region between the epidermal and dermal layers, and do not affect the stratum corneum unless the tumor has grown to the surface of the skin. These differences in tumor location within the multilayer structure of the skin is likely to be the reason behind our findings that the detection accuracy of BCC is higher for the non-invasive than the microinvasive electrodes, and the detection accuracy of MM appears to be higher for the microinvasive than the non-invasive electrodes.

The number of tumors in paper **V** was limited, in particular the number of MMs. This means that there are numerical limitations in order to avoid over-fitting of the algorithms. The LDA model was chosen to classify the lesions because of its simplicity and generality. However, LDA works best with highly clustered groups that are linearly related to each other, which is not the case in this study, as demonstrated in figure 33. This study provides evidence that the choice of probe – non-invasive or microinvasive – is application dependent, using general numerical methods, the same methods for both types of probes. If optimised separately, higher accuracy could be achieved for both, but then the comparison, which was the purpose of this paper, would not be as straightforward. If more cancer readings were available, more advanced and complex pattern recognition tools could have been tried, such as partial least squares regression (PLS) [32, 69], soft independent modelling of class analogy (SIMCA) [57], and artificial neural networks (ANN) [52, 98], which most likely would improve the detection accuracy of the technique.

The linear classifier used in paper **V** did not take into account that it is potentially lethal to miss a cancer in skin cancer screening, whereas it is, more or less, acceptable to misclassify a fraction of the benign lesions. The classification algorithm tried to find discriminant equations that maximised the total number of correct classifications in general, and did not account for the clinical considerations and consequences involved in skin cancer screening. Each measurement, $\mathbf{x}$, is classified to group y based on the outcome of the linear discriminant equation, $f(\mathbf{x})=\mathbf{w}'\mathbf{x}+b$, according to:

$$y = \begin{cases} \text{"benign" if } f(\mathbf{x}) \geq a \\ \text{"cancer" if } f(\mathbf{x}) < a \end{cases}$$

Hence, when the data, **x**, is projected onto the discriminant direction, **w**, the lesions are classified based on a simple cut-off, *a*. By varying the cut-off it is possible to adjust the discrimination to agree with the clinical considerations of skin cancer, i.e. to maximise the sensitivity at the price of a somewhat lower specificity. Moreover, ROC curves can be constructed by varying the cut-off, and thus a fair estimation of the accuracy, the area under ROC, can be used to compare the techniques in paper **V**, shown in figure 34. The ROC curves were calculated using cross-validation technique, and a random selection of 12.5% of the measurements were used as test set for each of the 8 cross-validation iterations. The cross-validation procedure was repeated 20 times to check the stability of the classification models. The median AUC of melanoma detection using microinvasive impedance PCA was 90.7%, and 96.5% for BCC detection using PCA and non-invasive impedance. The variation of the AUCs of the 20 cross-validation rounds decreased with increasing AUC. Cross-validation with random test sets will give a slightly different outcome each time, specially if the AUC is low because of poor separation between the groups – the SE of the AUC decrease with increasing area, as described in section 1.2.2.1, which means that the stability of the models increase with increasing separation.

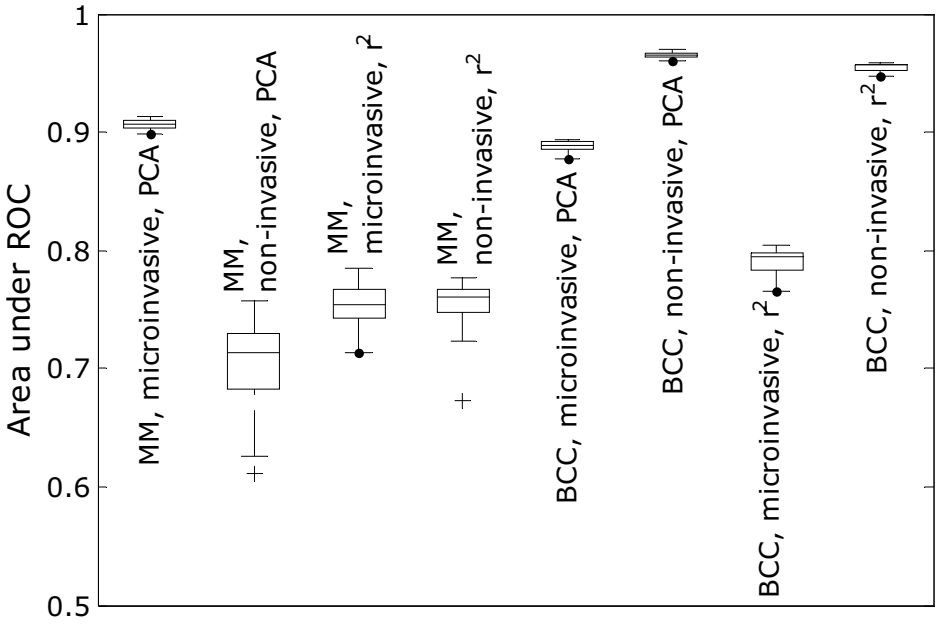

Figure 34. Box plots of the areas under ROC curves of cancer detection. The area under a ROC curve is an estimate of the overall accuracy in separating the cancers from the benign lesions. The figure shows the accuracy of the measurement techniques and data parameterisation of the two cancer types. The areas were estimated using cross-validation. To capture the variation, i.e. the stability, of the classification models, the cross-validation procedure was repeated 20 times, which is represented by the size (25, 50, and 75% percentiles) of the boxes.

5 GENERAL DISCUSSION

THIS project has been under development for several years, and the papers in this thesis reflect the progress. First it was demonstrated that there are statistically significant differences between reference skin and various lesion types [paper **II**]. A new version of the instrument, virtually immune to external electromagnetic interference, improved the signal-to-noise ratio and it was possible to use the electrical bio-impedance to distinguish common benign nevi from NMSC and MM with clinically relevant accuracy [paper **III**]. It is known that baseline impedance varies with many factors, e.g. body site [paper **I**], gender, age, season, and blood glucose concentration. These biological variations dilute the cancer signals in non-invasive impedance spectra, and hence impair the accuracy of cancer detection. A novel electrode system with spikes that penetrate the SC should reduce some of these variations [paper **IV**], and the performance of MM detection was improved by using this microinvasive electrode system [paper **V**].

In parts of this thesis, the aim was to distinguish NMSC and actinic keratoses from common trivial pigmented benign nevi. Trained general practitioners can separate them by visual screening, and the clinical relevance of this comparison may thus be limited. However, technically, our results demonstrate a significant potential of the method, despite the fact that the choice of lesions was motivated by experimental availability rather than clinical urgency.

The diameter of the outer electrode of the non-invasive probe is larger than most of the lesions in the studies. Measurements of small lesions will include impedance of both lesion and nearby skin, and the contribution of the nearby skin would thus dilute the lesion impedance. In [52] it was discussed that measurements of small lesions include impedance of both lesion and nearby skin, $Z = Z_{lesion} + Z_{skin}$, and the Z_{skin} should be reduced to improve the accuracy. In theory, the Z_{skin} proportion would increase with decreasing lesion diameter. The proportion Z_{skin} would also increase with decreasing

thickness of the lesion. Moreover, the 3d shape of the lesion would also influence the impedance; the Z_{skin} proportion would e.g. be higher for cone-shaped lesions than for half-sphere-shaped. Moreover, the proportion Z_{skin} would also increase with increasing depth penetration of the currents. It is easy to measure the diameter of the lesions on top of the skin, but the spatial factors affecting the Z_{skin} proportion are unknown unless the lesions are excised and measured, which is practically inapplicable, or visualised using e.g. ultrasound. Moreover, the exact depth penetration of currents is unknown. Hence, it is ambiguous to adjust the measured impedance with lesion size in order to eliminate or reduce the Z_{skin} contribution, which was proposed in [52], and thus it was found that simple normalisation using reference skin close to the lesion was better for skin cancer detection than adjusting the measured impedance with lesion size. The lesions included in our studies are obviously big enough to influence the pattern of the impedance spectra in a characteristic way. Of course there will be a lower limit that can be allowed in order to get data clearly above the noise level, but this is not sufficiently investigated at this point. It is possible to reduce the size of the electrode system somewhat to accommodate for smaller lesions but it must be kept in mind that the skin surface structure with its furrows and ridges sets a limit for meaningful reduction of the electrodes.

At this point, impedance of cutaneous lesions has been measured at a surgeon's clinic [Department of Surgery, Läkarmottagningen Hötorget, Stockholm, Sweden] for almost four years. Impedance spectra of thousands of lesions have been assessed. The experience of the personnel working with the measurements, both the operator and the highly experienced surgeon, is that plots of the raw impedance spectra are helpful in the screening process. They use the graphs as an aid when they sort out atypical lesions that should be excised and diagnosed by histopathology, i.e. they apply the technique in its intended use. This is not a scientific proof-of-principle, but it gives a good estimation of the practical usefulness of the technique. However, it takes time to learn how to interpret the raw spectra with the naked eye. Thus, the intention of this project is to convert the subjective experience of the personnel to an objective automatised screening tool for skin cancer that can be used by any medical personnel that can measure impedance.

Despite the remaining shortcomings, the technique seems at least as good as other techniques, and therefore clinically useful, although more data is needed to fulfil the regulatory requirements for a screening tool for skin cancer.

6 FUTURE STUDIES

THE purpose of this impedance and skin cancer project is, of course, to develop a diagnostic decision support tool that can be used clinically as an addition to classical visual screening. The papers **II**-**V** strongly indicate that the electrical impedance technique can be used to detect skin cancer, i.e. proof-of-principle has been achieved. However, before the technique can be used as a routine instrument in the clinics, additional studies are required. A large number of additional measurements of MM lesions is necessary to thoroughly validate the technique. Since the incidence of melanoma is low, extensive data collection is needed, preferably through a multi-centre study to accelerate data accumulation.

The accuracy of the gold standard for skin cancer diagnosis, the histopathological evaluation, is not 100%, and the accuracy of the impedance technique cannot be higher than the gold standard. Thus, further studies of lesions would preferably include at least three histopathologists diagnosing all lesions in order to increase the accuracy of the gold standard somewhat, and thereby facilitating fine-tuning of the impedance technique to higher accuracy.

Dysplastic nevi are non-malignant lesions that can progress to MM, they are potentially harmful lesions that sometimes are referred to as pre-cancerous, and hence it is clinically relevant to detect the dysplastic lesions [47]. Paper **II** demonstrates that there are statistically significant differences between reference skin and dysplastic nevi, and in [55] electrical impedance was used to distinguish between dysplastic and benign lesions. Thus, dysplastic nevi affect impedance spectra, and future studies on such lesions are motivated since a diagnostic decision support tool for dysplastic nevi is needed. Preliminary unpublished results indicate that microinvasive impedance of dysplastic nevi is even more overlapping with benign nevi than MM, as shown in figure 35.

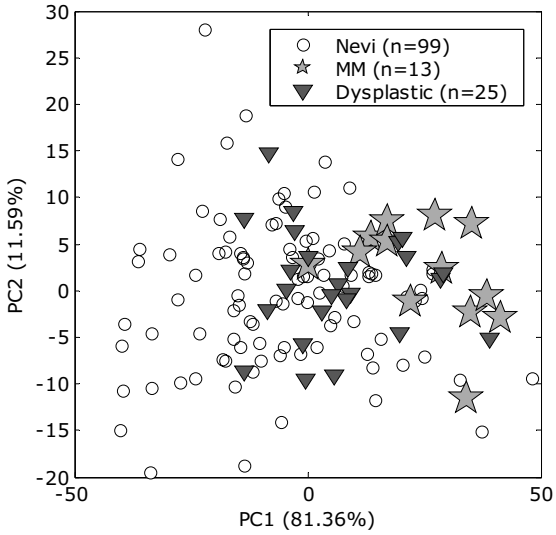

Figure 35. PCA scatter plot (PC1 vs. PC2) of microinvasive impedance of benign nevi, MM, and dysplastic nevi.

Moreover, when many impedance measurements of MM have been collected, advanced numerical pattern recognition methods can be used to detect the cancers, which should improve the accuracy. Possible numerical parameterisation tools that can be used include principal component analysis (PCA) [66], non-linear kernel PCA [114] (exemplified in figure 36), artificial self-organising maps (SOM) [116], and wavelets [117], and potentially useful numerical classifiers are linear discriminant analysis (LDA) [96], partial least squares regression (PLS) [118], soft independent modelling of class analogy (SIMCA) [100], and artificial neural networks (ANN) [119].

Apart from electrical impedance, there are other techniques that have been used to assess and detect skin cancer, such as near-infrared Fourier transform Raman spectroscopy [120], near infrared spectroscopy [121], laser Doppler perfusion [122, 123], dermoscopy [113], and high frequency ultrasound [124]. Combining impedance measurements with other techniques will increase the amount of cancer information, which most likely will improve the accuracy of skin cancer detection. A combination of multi-frequency total body bio-impedance and near infrared spectroscopy, described in [72], demonstrates the potential of combinations of physically independent non-invasive techniques.

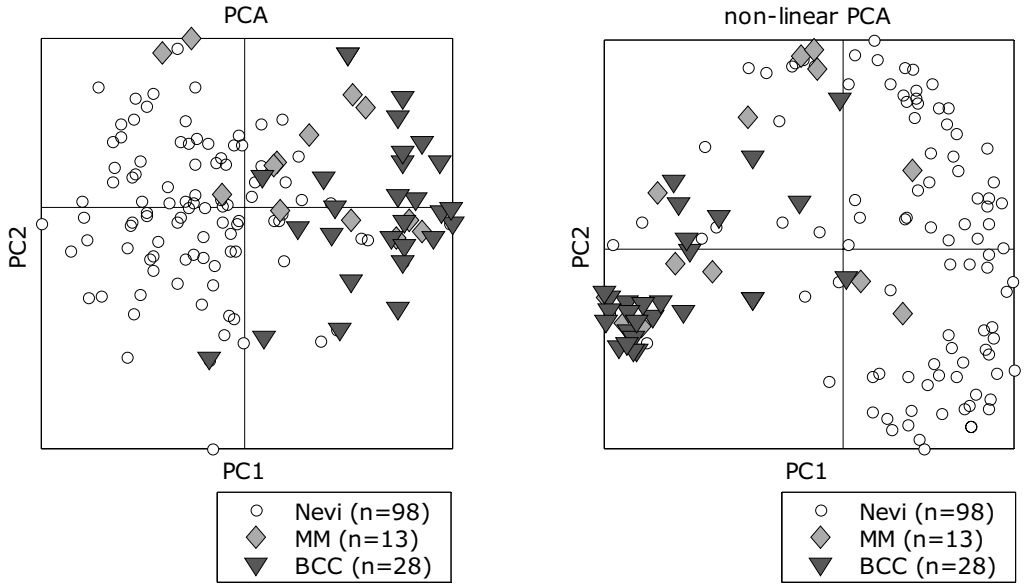

Figure 36. Scatter plots (PC1 vs. PC2) of regular linear PCA (left) and non-linear PCA (right) using Gaussian kernel [115]. The data used in this example are magnitude, phase, real part and imaginary parts of non-invasive and microinvasive measurements (1240 variables) from paper V. The degree of separation of the cancers and nevi seems to be higher in the non-linear case.

7 CONCLUSIONS

From the results of the studies in this thesis it can be concluded that:

I There are intra-individual non-invasive impedance variations within small areas on the body. This implies that utmost care in the study design is essential in order to facilitate observations of subtle reactions. Moreover, it is also implied that proper numerical analysis of multi-frequency impedance is crucial.

II There are statistically significant non-invasive impedance differences between reference skin and various skin lesions.

III Non-invasive impedance spectra measured with the SB II instrument can be used to distinguish NMSC from benign nevi and, to some degree, distinguish MM from nevi with clinically relevant accuracy.

IV Microinvasive impedance focuses on different skin layers than regular non-invasive impedance. Our results strongly suggest that the dominating contribution from the stratum corneum is substantially circumvented when using the microinvasive electrodes so that the α- and β-dispersions of living tissue are accentuated and biological variations, such as gender, age, and site-to-site variations, are reduced. The use of the microinvasive impedance electrodes is believed to enhance the clinical usefulness in several applications, in particular MM detection.

V The microinvasive electrodes seem better for MM detection than the regular non-invasive, and the non-invasive probes seem somewhat better for BCC detection. This indicates that the choice of electrode system is application dependent. In the general clinical context, use of both electrode systems may thus be indicated.

8 ACKNWOWLEDGEMENTS

THIS PhD project has been running for approximately four years – it has been a worthwhile and fun time, mainly due to all the persons involved. Hence, I would like to express my sincere gratitude to all those involved in and around this project, and in particular:

» Stig Ollmar, my main supervisor, for excellent supervision, scientific support, successful collaboration, and for making me see the fun in science generally
» Paul Geladi, chemometric supervisor, for showing me how to have fun with numbers
» Johan Hansson, clinical supervisor, for providing insights from the biological reality
» Lars Flening, company supervisor, for opening my eyes to the fun in realizing scientific discoveries
» the head of department, professor Håkan Elmqvist, for providing a fun and functional working environment
» Ingrid Nicander for clinical data, productive collaboration, and for making me see the fun in real-life clinical procedures
» the staff at Hötorgskliniken, Stockholm, who apparently found it fun to have us around
» all the volunteers providing me with not so fun biopsies
» the staff, co-workers, and associates at the division of Medical Engineering for a creative and fun atmosphere, for the discussions around the coffee table, and for travelling accompany at numerous hilarious conferences

Finally, I acknowledge my family and friends for their abiding support. Thank you!

This work was sponsored by SciBase AB, Huddinge, Sweden, the Knowledge Foundation, Sweden, Datex-Ohmeda/GE, Finland, the Swedish Foundation for Strategic Research, Sweden, and the Karolinska Institute, Stockholm, Sweden. The PhD project was carried out at the Division of Medical Engineering at the Karolinska Institute, Huddinge, Sweden, in collaboration with SciBase AB, Huddinge, Sweden, and the PhD Program in Biotechnology with an Industrial Focus at the Karolinska Institute, Stockholm, Sweden.

9 REFERENCES

[1] P. Åberg, P. Geladi, I. Nicander, and S. Ollmar, "Variation of skin properties within human forearms demonstrated by non-invasive detection and multi-way analysis," *Skin Res Technol*, vol. 8, pp. 194-201, 2002.

[2] P. Åberg, I. Nicander, U. Holmgren, P. Geladi, and S. Ollmar, "Assessment of skin lesions and skin cancer using simple electrical impedance indices," *Skin Res Technol*, vol. 9, pp. 257-61, 2003.

[3] P. Åberg, I. Nicander, J. Hansson, P. Geladi, U. Holmgren, and S. Ollmar, "Skin cancer identification using multi-frequency electrical impedance – a potential screening tool," *IEEE Trans Biomed Eng*, in press.

[4] P. Åberg, I. Nicander, and S. Ollmar, "Minimally invasive electrical impedance spectroscopy of skin exemplified by skin cancer assessments," in *Proceedings of the 25th Annual International Conference of the IEEE Engineering in Medicine and Biology Society, Vols 1-4 - a New Beginning for Human Health*, vol. 25, *Proceedings of Annual International Conference of the IEEE Engineering in Medicine and Biology Society*. New York: IEEE, 2003, pp. 3211-3214.

[5] P. Åberg, P. Geladi, I. Nicander, J. Hansson, U. Holmgren, and S. Ollmar, "Non-invasive and microinvasive electrical impedance spectra of skin cancer - a comparison between two techniques," *Skin Res Technol*, submitted.

[6] "Electrical Impedance," Encyclopædia Britannica. 2004. Encyclopædia Britannica Online. 6 Sept. 2004 <http://search.eb.com/eb/article?eu=32853>.

[7] K. R. Foster and H. P. Schwan, "Dielectric-Properties of Tissues and Biological-Materials - a Critical-Review," *Critical Reviews in Biomedical Engineering*, vol. 17, pp. 25-104, 1989.

[8] H. P. Schwan, "Electrical properties of tissue and cell suspensions," in *Advances in biological and medical physics*, vol. 5. New York: Academic press, 1957, pp. 147-224.

[9] S. Grimnes and Ø. G. Martinsen, *Bioimpedance and bioelectricity basics*. London (UK): Academic Press, 2000.

[10] U. G. Kyle, A. Piccoli, and C. Pichard, "Body composition measurements: interpretation finally made easy for clinical use," *Curr Opin Clin Nutr Metab Care*, vol. 6, pp. 387-93, 2003.

[11] B. H. Brown, "Electrical impedance tomography (EIT): a review," *J Med Eng Technol*, vol. 27, pp. 97-108, 2003.

[12] C. Longbottom and M. C. Huysmans, "Electrical measurements for use in caries clinical trials," *J Dent Res*, vol. 83 Spec No C, pp. C76-9, 2004.

[13] T. P. Habif, *Clinical dermatology: a color guide to diagnosis and therapy*, 2 ed. St. Louis, Missouri (US): The C.V. Mosby Company, 1990.

[14] H. Loffler, F. Dreher, and H. I. Maibach, "Stratum corneum adhesive tape stripping: influence of anatomical site, application pressure, duration and removal," *British Journal of Dermatology*, in press.

[15] C. Curdy, A. Naik, Y. N. Kalia, I. Alberti, and R. H. Guy, "Non-invasive assessment of the effect of formulation excipients on stratum corneum barrier function in vivo," *International Journal of Pharmaceutics*, vol. 271, pp. 251-256, 2004.

[16] I. Nicander, P. Åberg, and S. Ollmar, "Bioimpedance as a non-invasive method for measuring changes in skin," in *Handbook of non-invasive methods and the skin*, J. Serup, G. Jemec, and G. Grove, Eds. Boca Raton: CRC press, in press.

[17] S. Ollmar and I. Nicander, "Within and beyond the skin barrier as seen by electrical impedance," in *Bioengineering of the Skin: Water and the Stratum Corneum*, J. Fluhr, H. Maibach, E. Berardesca, and P. Elsner, Eds., 2 ed. Boca Raton, Fla: CRC Press, in press.

[18] Ø. G. Martinsen and S. Grimnes, "Facts and myths about electrical measurement of stratum corneum hydration state," *Dermatology*, vol. 202, pp. 87-9, 2001.

[19] I. Nicander, S. Ollmar, A. Eek, B. Lundh Rozell, and L. Emtestam, "Correlation of impedance response patterns to histological findings in irritant skin reactions induced by various surfactants," *Br J Dermatol*, vol. 134, pp. 221-8, 1996.

[20] I. Nicander and S. Ollmar, "Mild and below threshold skin responses to sodium lauryl sulphate assessed by depth controlled electrical impedance," *Skin Res Technol*, vol. 3, pp. 259-263, 1997.

[21] M. Nyren, L. Hagstromer, and L. Emtestam, "Instrumental measurement of the Mantoux test: differential effects of tuberculin and sodium lauryl sulphate on impedance response patterns in human skin," *Dermatology*, vol. 201, pp. 212-7, 2000.

[22] I. Nicander, P. Åberg, and S. Ollmar, "The use of different concentrations of betaine as a reducing irritation agent in soaps monitored visually and non-invasively," *Skin Res Technol*, vol. 9, pp. 43-9, 2003.

[23] I. Nicander, I. Rantanen, B. L. Rozell, E. Soderling, and S. Ollmar, "The ability of betaine to reduce the irritating effects of detergents assessed visually, histologically and by bioengineering methods," *Skin Res Technol*, vol. 9, pp. 50-8, 2003.

[24] I. Nicander, M. Nyrén, L. Emtestam, and S. Ollmar, "Baseline electrical impedance measurements at various skin sites related to age and sex," *Skin Res Technol*, vol. 3, pp. 252-258, 1997.

[25] I. Nicander and S. Ollmar, "Electrical impedance measurements at different skin sites related to seasonal variations," *Skin Res Technol*, vol. 6, pp. 81-86, 2000.

[26] L. Norlen, I. Nicander, B. Lundh Rozell, S. Ollmar, and B. Forslind, "Inter- and intra-individual differences in human stratum corneum lipid content related to physical parameters of skin barrier function in vivo," *J Invest Dermatol*, vol. 112, pp. 72-7, 1999.

[27] I. Nicander, L. Norlen, B. Forslind, and S. Ollmar, "Lipid content and electrical impedance," *Curr Probl Dermatol*, vol. 26, pp. 165-76, 1998.

[28] I. Nicander, L. Norlén, U. Brockstedt, B. Lundh-Rozell, B. Forslind, and S. Ollmar, "Electrical impedance and other physical parameters as related to lipid content of human stratum corneum," *Skin Res Technol*, vol. 4, pp. 213-221, 1998.

[29] U. Birgersson, F. Neiderud, P. Åberg, and S. Ollmar, "Blood glucose modulates impedance level," In proc. XII Intern Conf on Electrical Bio-Impedance & V Electrical Impedance Tomography, Gdansk (PL), pp. 153-156, 2004. ISBN 83-917681-6-3.

[30] H. R. Elden, *Method for non-invasive determination of glucose in body fluids*, USA: US patent 5890489, Jul. 30, 1996.

[31] I. Nicander and S. Ollmar, "Clinically normal atopic skin vs. non-atopic skin as seen through electrical impedance," *Skin Res Technol*, vol. 10, pp. 178-83, 2004.

[32] B. Lindholm-Sethson, S. Han, S. Ollmar, I. Nicander, G. Jonsson, F. Lithner, U. Bertheim, and P. Geladi, "Multivariate analysis of skin impedance data in long-term type 1 diabetic patients," *Chemometrics and Intelligent Laboratory Systems*, vol. 44, pp. 381-394, 1998.

[33] M. Gildemeister, "Über elektrischen Wiederstand, Kapazität und Polarisation der Haut," *Pflügers Arch für Physiol*, vol. 176, pp. 84-101, 1919.

[34] I. Nicander, *Electrical impedance related to experimentally induced changes of human skin and oral mucosa* (PhD thesis). Stockholm, Sweden: Karolinska Institutet, 1998.

[35] T. Yamamoto and Y. Yamamoto, "Electrical properties of the epidermal stratum corneum," *Med Biol Eng*, vol. 14, pp. 151-8, 1976.

[36] P. Griss, P. Enoksson, H. K. Tolvanen-Laakso, P. Merilainen, S. Ollmar, and G. Stemme, "Micromachined electrodes for biopotential measurements," *Journal of Microelectromechanical Systems*, vol. 10, pp. 10-16, 2001.

[37] I. Nicander, U. Holmgren, P. Åberg, and S. Ollmar, "Bioimpedance of different skin tumours - clinical tricks and treats," In proc. XII Intern Conf on Electrical Bio-Impedance & V Electrical Impedance Tomography, Gdansk (PL), pp. 99-102, 2004. ISBN 83-917681-6-3.

[38] S. Ollmar, I. Nicander, and P. Åberg, "Skin bioimpedance - on the outside and inside out," In proc. XII Intern Conf on Electrical Bio-Impedance & V Electrical Impedance Tomography, Gdansk (PL), pp. 343-346, 2004. ISBN 83-917681-6-3.

[39] T. L. Diepgen and V. Mahler, "The epidemiology of skin cancer," *Br J Dermatol*, vol. 146 Suppl 61, pp. 1-6, 2002.

[40] R. M. Shelton, "A review and atlas for the medical provider," *Mount Sinai Journal of Medicine*, vol. 68, pp. 243-252, 2001.

[41] T. R. Humphreys, "Skin cancer: recognition and management," *Clin Cornerstone*, vol. 4, pp. 23-32, 2001.

[42] E. Podczaski and J. Cain, "Cutaneous malignant melanoma," *Clinical Obstetrics and Gynecology*, vol. 45, pp. 830-843, 2002.

[43] C. S. Wong, R. C. Strange, and J. T. Lear, "Basal cell carcinoma," *Bmj*, vol. 327, pp. 794-8, 2003.

[44] G. Saldanha, A. Fletcher, and D. N. Slater, "Basal cell carcinoma: a dermatopathological and molecular biological update," *Br J Dermatol*, vol. 148, pp. 195-202, 2003.

[45] T. H. Nguyen and D. Q. Ho, "Nonmelanoma skin cancer," *Curr Treat Options Oncol*, vol. 3, pp. 193-203, 2002.

[46] W. Fu and C. J. Cockerell, "The actinic (solar) keratosis - A 21st-century perspective," *Archives of Dermatology*, vol. 139, pp. 66-70, 2003.

[47] J. M. Naeyaert and L. Brochez, "Clinical practice. Dysplastic nevi," *N Engl J Med*, vol. 349, pp. 2233-40, 2003.

[48] L. Izikson, A. J. Sober, M. C. Mihm, Jr., and A. Zembowicz, "Prevalence of melanoma clinically resembling seborrheic keratosis: analysis of 9204 cases," *Arch Dermatol*, vol. 138, pp. 1562-6, 2002.

[49] J. C. Pierson, "Dermatofibroma," e-medicine. 16 Sept. 2004 <http://www.emedicine.com/derm/topic96.htm>, 2004.

[50] M. C. Oliviero, "How to diagnose malignant melanoma," *Nurse Pract*, vol. 27, pp. 26-7, 31-5; quiz 36-7, 2002.

[51] M. Helfand, S. M. Mahon, K. B. Eden, P. S. Frame, and C. T. Orleans, "Screening for skin cancer," *Am J Prev Med*, vol. 20, pp. 47-58, 2001.

[52] R. Dua, D. G. Beetner, W. V. Stoecker, and D. C. Wunsch, 2nd, "Detection of basal cell carcinoma using electrical impedance and neural networks," *IEEE Trans Biomed Eng*, vol. 51, pp. 66-71, 2004.

[53] D. G. Beetner, S. Kapoor, S. Manjunath, X. Zhou, and W. V. Stoecker, "Differentiation among basal cell carcinoma, benign lesions, and normal skin using electric impedance," *IEEE Trans Biomed Eng*, vol. 50, pp. 1020-5, 2003.

[54] L. Emtestam, I. Nicander, M. Stenstrom, and S. Ollmar, "Electrical impedance of nodular basal cell carcinoma: a pilot study," *Dermatology*, vol. 197, pp. 313-6, 1998.

[55] Y. A. Glickman, O. Filo, M. David, A. Yayon, M. Topaz, B. Zamir, A. Ginzburg, D. Rozenman, and G. Kenan, "Electrical impedance scanning: a new approach to skin cancer diagnosis," *Skin Res Technol*, vol. 9, pp. 262-8, 2003.

[56] P. Åberg, I. Nicander, U. Holmgren, J. Hansson, and S. Ollmar, "Bioimpedance as a potential diagnostic decision tool for skin neoplasms," In proc. 2nd European Medical and Biological Engineering Conference, Vienna, pp. 80-81, 2002. ISBN 3-901351-62-0.

[57] P. Åberg, I. Nicander, J. Hansson, U. Holmgren, and S. Ollmar, "Skin bioimpedance - electronic views of malignancies," In proc. XII Intern Conf on Electrical Bio-Impedance & V Electrical Impedance Tomography, Gdansk (PL), pp. 79-82, 2004. ISBN 83-917681-6-3.

[58] H. A. L. Kiers, "Towards a standardized notation and terminology in multiway analysis," *Journal of Chemometrics*, vol. 14, pp. 105-122, 2000.

[59] K. S. Cole, "Permeability and impermeability of cell membranes for ions," *Cold Spring Harbor Sympos Quant Biol*, vol. 8, pp. 110-122, 1940.

[60] S. Ollmar and I. Nicander, "Information in multi frequency measurement of intact skin," *Innov Tech Biol Med*, vol. 16, pp. 745-751, 1995.

[61] S. Ollmar, "Methods of information extraction from impedance spectra of biological tissue, in particular skin and oral mucosa - a critical review and suggestions for the future," *Bioelectrochemistry and Bioenergetics*, vol. 45, pp. 157-160, 1998.

[62] M. Nyren, L. Hagströmer, and L. Emtestam, "On Assessment of Skin Reactivity Using Electrical Impedance," *Ann NY Acad Sci*, vol. 873, pp. 214-220, 1999.

[63] S. Ollmar, I. Nicander, J. Ollmar, and L. Emtestam, "Information in full and reduced data sets of electrical impedance spectra from various skin conditions, compared using a holographic neural network," *Med Biol Eng Comput*, vol. 35, pp. 415-9, 1997.

[64] S. Ollmar, "Making electronic biopsies into a viable future for non-invasive diagnostics with electrical impedance," *Med Biol Eng Comput*, vol. 37, Suppl 2, pp. 116-117, 1999.

[65] I. Lackovic, Z. Stare, and T. Protulipac, "On the applicability of electrical impedance indices to characterize the condition of the oral mucosa," In proc. Fifth International Conference on Simulations in Biomedicine, Ljubljana, Slovenia, pp. 421-430, 2003. ISBN 1-85312-965-8.

[66] S. Wold, K. Esbensen, and P. Geladi, "Principal component analysis," *Chemometrics and Intelligent Laboratory Systems*, vol. 2, pp. 37-52, 1987.

[67] K. Pearson, "On lines and planes of closest fit to systems of points in space," *Philosophical Magazine*, vol. 2, pp. 559-572, 1901.

[68] H. Martens and T. Naes, *Multivariate Calibration*. Chichester (UK): Wiley, 1989.

[69] L. Eriksson, E. Johanssson, N. Kettaneh-Wold, and S. Wold, *Multi- and megavariate data analysis. Principles and Applications*. Umeå (SE): Umetrics AB, 2001.

[70] I. T. Jolliffe, *Principal Component Analysis*, 2nd ed. New York: Springer, 2002.

[71] B. Lindholm-Sethson, P. Geladi, and A. Nelson, "Interaction with a phospholipid, monolayer on a mercury electrode - Multivariate

analysis of impedance data," *Analytica Chimica Acta*, vol. 446, pp. 121-131, 2001.

[72] J. Nyström, B. Lindholm-Sethson, L. Stenberg, S. Ollmar, J. W. Eriksson, and P. Geladi, "Combined near-infrared spectroscopy and multifrequency bio-impedance investigation of skin alterations in diabetes patients based on multivariate analyses," *Med Biol Eng Comput*, vol. 41, pp. 324-9, 2003.

[73] L. Guerrero, I. Gobantes, M. A. Oliver, J. Arnau, M. D. Guardia, J. Elvira, P. Riu, N. Grebol, and J. M. Monfort, "Green hams electrical impedance spectroscopy (EIS) measures and pastiness prediction of dry cured hams," *Meat Science*, vol. 66, pp. 289-294, 2004.

[74] H. Sorgatz, "Components of skin impedance level," *Biol Psychol*, vol. 6, pp. 121-5, 1978.

[75] R. Bro, "Exploratory study of sugar production using fluorescence spectroscopy and multi-way analysis," *Chemometrics and Intelligent Laboratory Systems*, vol. 46, pp. 133-147, 1999.

[76] C. M. Andersen and R. Bro, "Practical aspects of PARAFAC modeling of fluorescence excitation-emission data," *Journal of Chemometrics*, vol. 17, pp. 200-215, 2003.

[77] R. Bro, *Multi-way analysis in the food industry. Models, algorithms and applications* (PhD thesis). Royal Veterinary and Agricultural University, Denmark, 1998.

[78] L. R. Tucker, "Some mathematical notes on three-mode factor analysis," *Psychometrika*, vol. 31, pp. 279-311, 1966.

[79] R. Bro and H. A. L. Kiers, "A new efficient method for determining the number of components in PARAFAC models," *Journal of Chemometrics*, vol. 17, pp. 274-286, 2003.

[80] R. A. Harshman, "Foundations of the PARAFAC procedure: Model and conditions for an 'explanatory' multi-mode factor analysis," *UCLA Working Papers in phonetics*, vol. 16, pp. 1-84, 1970.

[81] J. D. Carrol and J. Chang, "Analysis of individual differences in multidimensional scaling via an N-way generalization of the Eckart-Young decomposition," *Psychometrika*, vol. 35, pp. 283-319, 1970.

[82] C. Andersson and R. Bro, "Special issue: Multiway analysis," *Journal of Chemometrics*, vol. 14, pp. 103-103, 2000.

[83] R. Bro, "PARAFAC. Tutorial and applications," *Chemometrics and Intelligent Laboratory Systems*, vol. 38, pp. 149-171, 1997.

[84] A. Smilde, R. Bro, and P. Geladi, *Multi-way Analysis : Applications in the Chemical Sciences*. Chichester (UK): John Wiley & Sons, 2004.

[85] P. Geladi and P. Åberg, "Three-way modelling of a batch organic synthesis process monitored by near infrared spectroscopy," *Journal of near Infrared Spectroscopy*, vol. 9, pp. 1-9, 2001.

[86] R. Bro, N. D. Sidiropoulos, and G. B. Giannakis, "A Fast Least Squares Algorithm for Separating Trilinear Mixtures," In proc. ICA99 Int. Workshop on Independent Component Analysis and Blind Signal Separation, Aussois, France, pp. 289-294, 1999.

[87] K. Woods, M. Y. Sallam, and K. W. Bowyer, "Evaluating Detection Algorithms," in *Image-Processing Techniques for Tumor Detection*, R. N. Strickland, Ed. New York, NY, USA: Marcel Dekker Incorporated, 2002.

[88] J. A. Hanley and B. J. McNeil, "The meaning and use of the area under a receiver operating characteristic (ROC) curve," *Radiology*, vol. 143, pp. 29-36, 1982.

[89] M. H. Zweig and G. Campbell, "Receiver-operating characteristic (ROC) plots: a fundamental evaluation tool in clinical medicine," *Clin Chem*, vol. 39, pp. 561-77, 1993.

[90] M. Greiner, D. Pfeiffer, and R. D. Smith, "Principles and practical application of the receiver-operating characteristic analysis for diagnostic tests," *Prev Vet Med*, vol. 45, pp. 23-41, 2000.

[91] B. H. Brown, J. A. Tidy, K. Boston, A. D. Blackett, R. H. Smallwood, and F. Sharp, "Relation between tissue structure and imposed electrical current flow in cervical neoplasia," *Lancet*, vol. 355, pp. 892-895, 2000.

[92] R. Smallwood, F. Hamdy, A. Keshtkar, B. Wilkinson, J. Lee, and R. Azzouzi, "Electrical impedance spectroscopy identifies malignant areas in the bladder," In proc. XII Intern Conf on Electrical Bio-Impedance & V Electrical Impedance Tomography, Gdansk (PL), pp. 425-428, 2004. ISBN 83-917681-6-3.

[93] S. Mika, *Kernel Fisher Discriminants* (PhD thesis). Berlin: der Technischen Universität Berlin, 2002.

[94] N. H. Timm, *Applied Multivariate Analysis*. New York: Springer-Verlag, 2002.

[95] Y. Mallet, D. Coomans, and O. deVel, "Recent developments in discriminant analysis on high dimensional spectral data," *Chemometrics and Intelligent Laboratory Systems*, vol. 35, pp. 157-173, 1996.

[96] W. Wu, Y. Mallet, B. Walczak, W. Penninckx, D. L. Massart, S. Heuerding, and F. Erni, "Comparison of regularized discriminant analysis, linear discriminant analysis and quadratic discriminant

analysis, applied to NIR data," *Analytica Chimica Acta*, vol. 329, pp. 257-265, 1996.

[97] U. Indahl, N. Sahni, B. Kirkhus, and N. Tormod, "Multivariate strategies for classification based on NIR-spectra-with application to mayonnaise," *Chemometrics and Intelligent Laboratory Systems*, vol. 49, pp. 19-31, 1999.

[98] Y. Tominaga, "Comparative study of class data analysis with PCA-LDA, SIMCA, PLS, ANNs, and k-NN," *Chemometrics and Intelligent Laboratory Systems*, vol. 49, pp. 105-115, 1999.

[99] R. Franke, S. Dove, and A. Gruska, "Physicochemical properties and drug action: alternative QSAR methods," in *Advanced Drug Design & Development: A Medicinal Chemistry Approach*, P. H. Kourounakis, Ed. Old Tappan, NJ, USA: Prentice-Hall, 1994.

[100] S. Wold, "Pattern recognition by means of disjoint principal components models," *Pattern Recognition*, vol. 8, pp. 127-139, 1976.

[101] R. De Maesschalck, A. Candolfi, D. L. Massart, and S. Heuerding, "Decision criteria for soft independent modelling of class analogy applied to near infrared data," *Chemometrics and Intelligent Laboratory Systems*, vol. 47, pp. 65-77, 1999.

[102] B. M. Wise and N. B. Gallagher, *PLS Toolbox Version 2.0 for use with MATLAB*. Manson, WA, USA: Eigenvector Research Inc., 1998.

[103] G. E. Nilsson, *On the measurement of evaporative water loss. Methods and clinical applications* (PhD thesis). Linköping, Sweden: Linköping Medical University, 1977.

[104] J. Pinnagoda, R. A. Tupker, T. Agner, and J. Serup, "Guidelines for Transepidermal Water-Loss (TEWL) Measurement - a Report from the Standardization-Group-of-the European-Society-of-Contact-Dermatitis," *Contact Dermatitis*, vol. 22, pp. 164-178, 1990.

[105] C. A. Andersson and R. Bro, "The N-way Toolbox for MATLAB," *Chemometrics and Intelligent Laboratory Systems*, vol. 52, pp. 1-4, 2000.

[106] A. Björnberg, *Skin reactions to primary irritants in patients with hand eczema: an investigation with matched controls* (PhD Thesis). Göteborg, Sweden: Sahlgrenska Sjukhuset, 1968.

[107] L. Rodrigues and L. M. Pereira, "Basal transepidermal water loss: right/left forearm difference and motoric dominance," *Skin Res Technol*, vol. 4, pp. 135-137, 1998.

[108] P. G. M. Vandervalk and H. I. Maibach, "Potential for Irritation Increases from the Wrist to the Cubital Fossa," *Br J Dermatol*, vol. 121, pp. 709-712, 1989.

[109] E. Tur, H. Maibach, and R. H. Guy, "Spatial variability of vasodilatation in human forearm skin," *Br J Dermatol*, vol. 113, pp. 197-203., 1985.

[110] M. K. Robinson, "Intra-individual variations in acute and cumulative skin irritation responses," *Contact Dermatitis*, vol. 45, pp. 75-83, 2001.

[111] S. M. Cooper and F. Wojnarowska, "The accuracy of clinical diagnosis of suspected premalignant and malignant skin lesions in renal transplant recipients," *Clinical and Experimental Dermatology*, vol. 27, pp. 436-438, 2002.

[112] A. Offidani, O. Simonetti, M. L. Bernardini, A. Alpagut, A. Cellini, and G. Bossi, "General practitioners' accuracy in diagnosing skin cancers," *Dermatology*, vol. 205, pp. 127-130, 2002.

[113] H. Kittler, H. Pehamberger, K. Wolff, and M. Binder, "Diagnostic accuracy of dermoscopy," *Lancet Oncology*, vol. 3, pp. 159-165, 2002.

[114] B. Schölkopf, A. Smola, and K. R. Müller, "Nonlinear component analysis as a kernel eigenvalue problem," *Neural Computation*, vol. 10, pp. 1299-1319, 1998.

[115] V. Franc and V. Hlavac, *Statistical Pattern Recognition Toolbox for Matlab. User's guide*. Prague, Czech Republic: Center for Machine Perception, Department of Cybernetics, Faculty of Electrical Engineering, Czech Technical University, Technicka 2, 2004.

[116] T. Kohonen, E. Oja, O. Simula, A. Visa, and J. Kangas, "Engineering applications of the self-organizing map," *Proceedings of the IEEE*, vol. 84, pp. 1358-1384, 1996.

[117] S. Mallat, *A Wavelet Tour of Signal Processing*. New York (US): Academic Press, 1998.

[118] P. Geladi and B. R. Kowalski, "Partial Least-Squares Regression - a Tutorial," *Analytica Chimica Acta*, vol. 185, pp. 1-17, 1986.

[119] K. Gurney, *An introduction to neural networks*. London: Routledge, 1997.

[120] M. Gniadecka, P. A. Philipsen, S. Sigurdsson, S. Wessel, O. F. Nielsen, D. H. Christensen, J. Hercogova, K. Rossen, H. K. Thomsen, R. Gniadecki, L. K. Hansen, and H. C. Wulf, "Melanoma diagnosis by Raman spectroscopy and neural networks: structure alterations in proteins and lipids in intact cancer tissue," *J Invest Dermatol*, vol. 122, pp. 443-9, 2004.

[121] L. M. McIntosh, R. Summers, M. Jackson, H. H. Mantsch, J. R. Mansfield, M. Howlett, A. N. Crowson, and J. W. Toole, "Towards

non-invasive screening of skin lesions by near-infrared spectroscopy," *J Invest Dermatol*, vol. 116, pp. 175-81, 2001.

[122] E. Tur and S. Brenner, "Cutaneous blood flow measurements for the detection of malignancy in pigmented skin lesions," *Dermatology*, vol. 184, pp. 8-11, 1992.

[123] M. A. Ilias, K. Wårdell, M. Stucker, C. Anderson, and E. G. Salerud, "Assessment of pigmented skin lesions in terms of blood perfusion estimates," *Skin Res Technol*, vol. 10, pp. 43-49, 2004.

[124] B. Bessoud, N. Lassau, S. Koscielny, C. Longvert, M. F. Avril, P. Duvillard, V. Rouffiac, J. Leclere, and A. Roche, "High-frequency sonography and color Doppler in the management of pigmented skin lesions," *Ultrasound Med Biol*, vol. 29, pp. 875-9, 2003.